Journal of Materials Chemistry B

Accepted Manuscript

ROYAL SOCIETY OF CHEMISTRY

www.rsc.org/materialsB

Gold-graphene nanocomposites for sensing and biomedical applications

Kostiantyn Turcheniuk, Rabah Boukherroub and Sabine Szunerits*

Institut d'Electronique, de Microélectronique et de Nanotechnologie (IEMN, UMR CNRS 8520), Université Lille1, Cité Scientifique, Avenue Poincaré, 59652 Villeneuve d'Ascq, France

Abstract

Recent developments in materials science and nanotechnology have propelled the development of a plethora of materials with unique chemical and physical properties for biomedical applications. Graphitic nanomaterials such as carbon nanotubes, fullerenes and, more recently, graphene oxide (GO) and reduced graphene oxide (rGO), have gained a great deal of interest in this domain. Beside the exceptional physico-chemical features of these materials, they can be easily produced in good quantities. Moreover, the presence of abundant functional groups on their surface and good biocompatibility make them highly suitable for biomedical applications. Many research groups have utilized GO and rGO nanocargos to effectively deliver insoluble drugs, nucleic acids and other molecules into cells for bioimaging and therapeutic purposes. Gold nanostructures (Au NSs), on the other hand, have also generated a great attention owing to their applications in biomedical field, organic catalysis, etc. Loading of GO and rGO sheets with Au NSs generates a new class of functional materials with improved properties and thus provides new opportunities of such hybrid materials for catalytic biosensing and biomedical applications. This review article is aimed at providing an insight on the important features of gold-graphene nanocomposites, the current research activities related to the different synthetic routes to produce these nanocomposites, and their potential applications in sensing and biomedical therapy, notably photothermal therapy (PTT).

***Keywords**: graphene, gold nanoparticles, nanocomposites, photothermal therapy, cancer*

1. Introduction

Recent years have witnessed tremendous progress made in the design and use of nanomaterials geared towards biomedical and biological applications. Among these nanomaterials, gold nanostructures (Au NSs) have especially been intensively studied (**Figure 1A**). Au NSs of different shapes and sizes can be easily prepared using solution-based techniques, have low toxicity and can be readily attached to molecules of biological relevance and interest. They are, therefore, well-suited for a wide range of biological applications comprising genomics, biosensors, immunoanalysis, detection and photothermolysis of microorganisms and cancer cells, targeted delivery of drugs, DNA and antigens as well as optical bioimaging. It has been argued that Au NSs could be used in fact in almost all medical applications such as diagnostics, therapy, prevention, and hygiene.[1, 2]

The exceptional optical properties of Au NSs, including large optical field enhancements and their addressability via spectroscopic techniques have made them of particular interest as labels and for biosensing. The optical properties are dominated by the excitation of collective oscillations of the nanoparticles' conduction band electrons, called localized surface plasmon resonances (LSPR), by the incoming electromagnetic waves.[3, 4] At the LSPR, the incoming light is absorbed or scattered by the Au NSs, and concurrently, there is an electromagnetic field enhancement close to the surface of the particle. The position of the plasmonic resonance depends on the particle size, shape, composition, interparticle distance as well as the dielectric environment. As seen in **Figure 1B**, spherical Au NPs of 20 nm in diameter show a LSPR resonance at ≈520 nm, while Au nanorods are characterized by two LSPR bands at 522 and 736 nm, respectively.[5] As the position of the LSPR band is in addition influenced by the refractive index of the surrounding medium sensing, such structures have been intensively used to detect molecular-binding events in the nano-environment of the particle.[3, 5-7]

The other way to employ Au NPs for sensing is to use discrete particle aggregation in response to biological elements, which results in a measurable color change. These colorimetric sensing systems exhibited relatively low detection limits with a high degree of sensitivity.[8, 9] The use of colloidal Au NPs as staining agents has become a standard procedure in biological microscopy and several reviews have discussed the use of Au NPs in a variety of diagnostic and therapeutic applications.[8, 10-12]

However, the use of as-synthesized Au NPs in biological systems is limited due by the particle instability and nonspecific binding. These limitations are even increasingly pronounced in high ionic strength media, such as those used for biological assays. The particle aggregation depends strongly on the type of ligand used to passivate the

nanoparticles' surface. The ligands can be displaced or even cross-linked due to the multitude of ionic species present in solution. Care has, in addition, to be paid to the biocompatibility of the particle ligand. For instance, cetyltrimethylammonium bromide (CTAB) modified gold nanorods (Au NRs) can be routinely prepared and display good colloidal dispersibility and stability. However, one of the major concerns is related to the cytotoxicity of the surfactant, CTAB, used to stabilize the particles. CTAB molecules can induce cytotoxicity by disrupting cellular membranes (**Figure 1C**).[13] CTAB is not only toxic to cells, but also very difficult to remove completely.[14, 15] In addition, CTAB-coated Au NRs lack targeting capabilities, something of critical importance for active targeting of cancer cells, pathogens, etc.

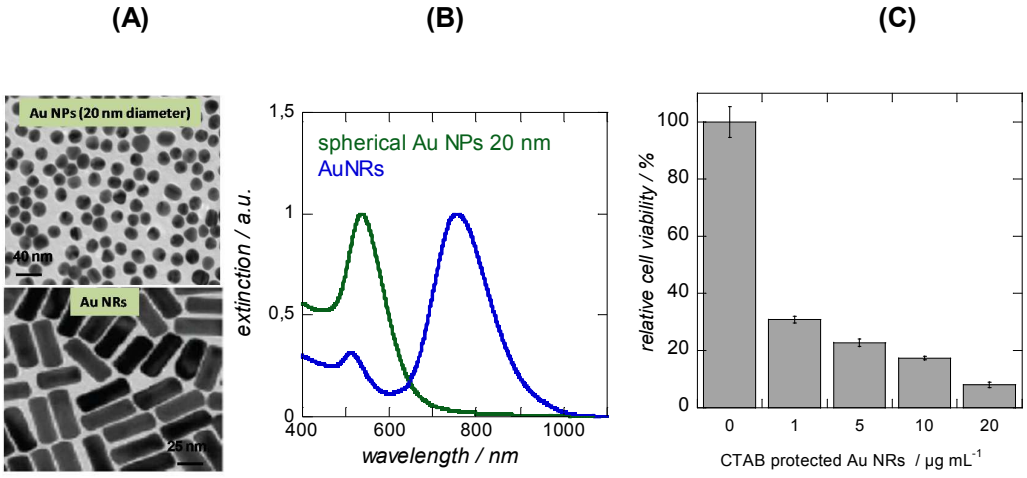

Figure 1. (A) TEM images of Au nanostructures; (B) Optical extinction spectra of citrate-capped spherical Au nanoparticles (green) and Au nanorods (blue); (C) Relative cell viability of MDA-MB-231 cells for different concentrations of CTAB coated Au NRs.[16]

Since the synthesis methodologies of Au NSs of different sizes, shapes, and surface chemistries are fairly mature, the current efforts for performance enhancement are moving towards the construction of novel Au NPs-based assemblies. An emerging method that has shown great promise involves the use of carbon nanoshells and carbon-based nanomatrices to encapsulate and to embed the Au NPs.[17, 18] A more recently discovered carbon-based material is graphene.[19, 20] Graphene is a sheet of two-dimensional (2D) single layer sp^2 hybridized carbon atoms with exceptional electrical, optical, thermal and mechanical properties. Since its discovery by Geim and co-workers in 2004, research on graphene has increased in an exceptional rate exploring different properties and applications ranging from electronic and optoelectronic devices to photoconductive materials in solar cells and others. With the rapid development of synthetic methods and functionalization approaches of

graphene oxide (GO), a highly oxidized form of graphene consisting of single atom-thick layers of graphene sheets with carboxylic acid, epoxide and hydroxyl groups in the plane, its outstanding potential for biomedical applications such as bioimaging, drug delivery and tissue engineering,[21] as well as biosensing[22, 23] have been exploited. However, the use of GO and reduced graphene oxide (rGO), obtained by reductive treatment of GO, in the biomedical field is relatively new. It started with the seminal report on the use of GO as an efficient nanocarrier for drug delivery by Dai et al. in 2008.[24] Since then a lot of interesting work has been carried out to explore the use of graphene and particular GO and rGO for biomedical applications.[25]

Having said that, a number of reports have demonstrated lately that graphene-Au NPs hybrid structures can act synergistically to offer a number of unique physicochemical properties.[22] In this respect, electronic applications have been the first and most popular ones of graphene-based materials due to the high electron mobility of graphene, and graphene/Au NPs hybrids have shown their interest by reducing the sheet resistances of rGO-based devices.[26] Moreover, the combination of Au NSs with graphene sheets can result in a positive synergetic effect and made pronounced impact in the biomedical and biosensing fields.[27]

This review chapter is focused on the description of the synthetic aspects of Au NSs wrapped with carbon-based materials, in particular graphene derivatives and the potential applications of the resulting Au NSs-graphene nanocomposites in biomedical field. The number of publications based on GO/Au NPs and rGO/Au NPS hybrids from 2009 - 2014 shows a steady increase (**Figure 2**). It is hoped that this review article will help in generating higher interest in the wider use graphene/Au NPs hybrids in biomedical and biological fields.

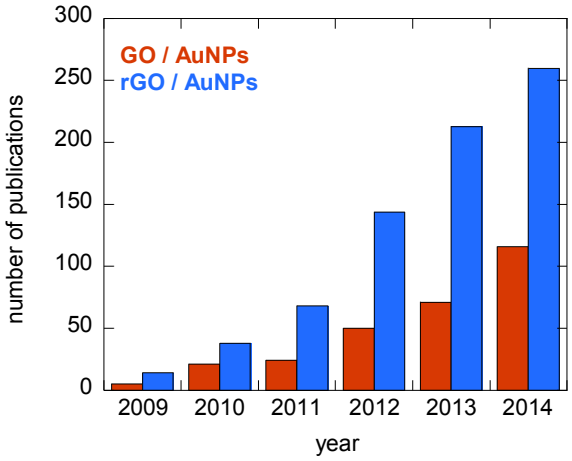

Figure 2: Number of articles published from 2009 -2014 according to Scopus on GO/Au NPS (red) and rGO/Au NPs (blue) hybrids for biomedical-related research.

We will start the review with a detailed description of the currently available procedures for the fabrication of GO, rGO and graphene wrapped Au NSs, followed by approaches to embed Au NSs onto graphene-based nanosheets. A detailed discussion on the application of the different hybrid structures for drug/gene delivery, photothermal therapy, electrochemical sensing and bioimaging. The review is concluded with some perspectives in the field.

2. Preparation of GO and its properties

Graphene oxide (GO) and reduced graphene oxide (rGO) are emerging materials for biomedical applications owing to their attractive physico-chemical properties. GO can be prepared in bulk quantities through extensive oxidation/exfoliation of graphite (**Figure 3A)**.[28] Upon oxidation, hydrophilic groups such as hydroxyl, carbonyl, and epoxy groups are introduced onto the surface of GO sheets. The presence of these oxygen-containing groups makes GO stably suspended in pure water for some time yet GO sheets tend to aggregate in salt- or protein-rich solutions such as cell medium and serum (**Figure 3B**).[24] Furthermore, cytotoxicity tests have shown that GO exhibits a certain concentration dependent toxicity to cells (**Figure 3B**).[29]

In recent years, extensive efforts have been devoted to the preparation of GO with good dispersibility in various aqueous media. Two approaches have been developed to produce homogenous and stable GO dispersions in solution. In the first strategy, covalent bonds are formed between the pending functional groups of GO and biocompatible polymers (**Figure 3C**). Due to its minimal toxicity, biocompatibility, protein resistance and good solubility in water and other common solvents, poly(ethylene glycol) (PEG) has become the reagent of choice for the covalent functionalization of GO. The polymer-functionalized GO sheets were not noticeably toxic *in vitro* and *in vivo* at the tested doses.[30] Dai et al. initially produced PEG-functionalized GO as a nanocarrier to load anticancer drugs via non-covalent physisorption and studied its cellular uptake.[24, 31] It was demonstrated that PEG-modified GO was biocompatible without obvious toxicity and could be loaded with aromatic anticancer drugs with high efficiency. Indeed [21] The other approach to prepare stable GO dispersions utilizes non-covalent functionalization. High molecular weight surfactants such as Pluronic has been used to produce stable GO dispersions in water through micelle encapsulation.[32] The use of sodium salt of pyrene butyric acid has also been reported to form stable GO dispersion in water through $\pi-\pi$ stacking interaction between pyrene moieties and π–orbitals of GO (**Figure 3C**).[33] Hu et al proposed a electrostatic self-assembly strategy for the formation of dispersable GO–AuNRs, where poly (*N*-vinyl-2-pyrrolidone) (PVP) served as stabilizing surfactant to avoid the aggregations of GO sheets (**Figure 3C**).[34]

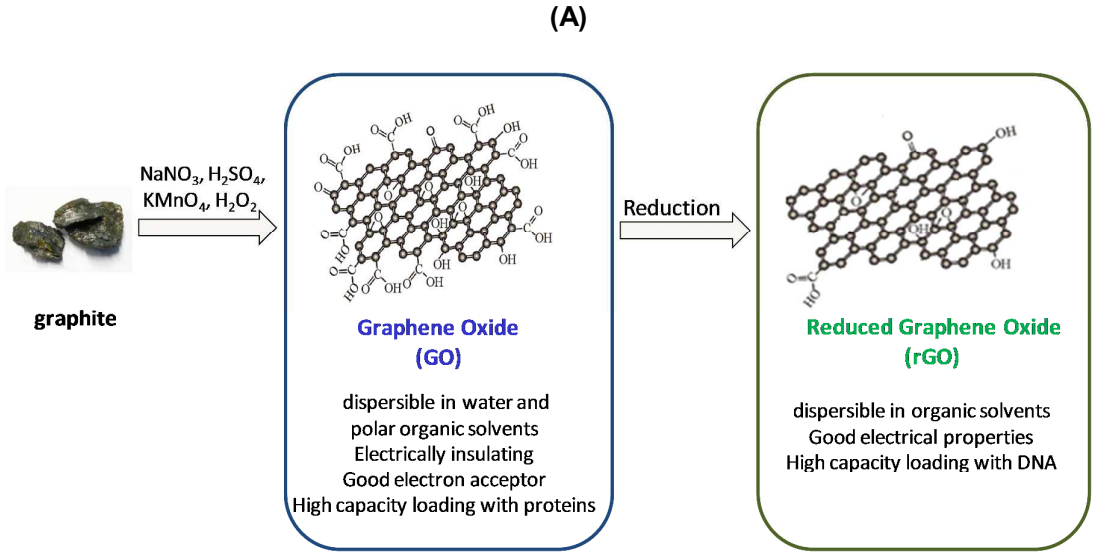

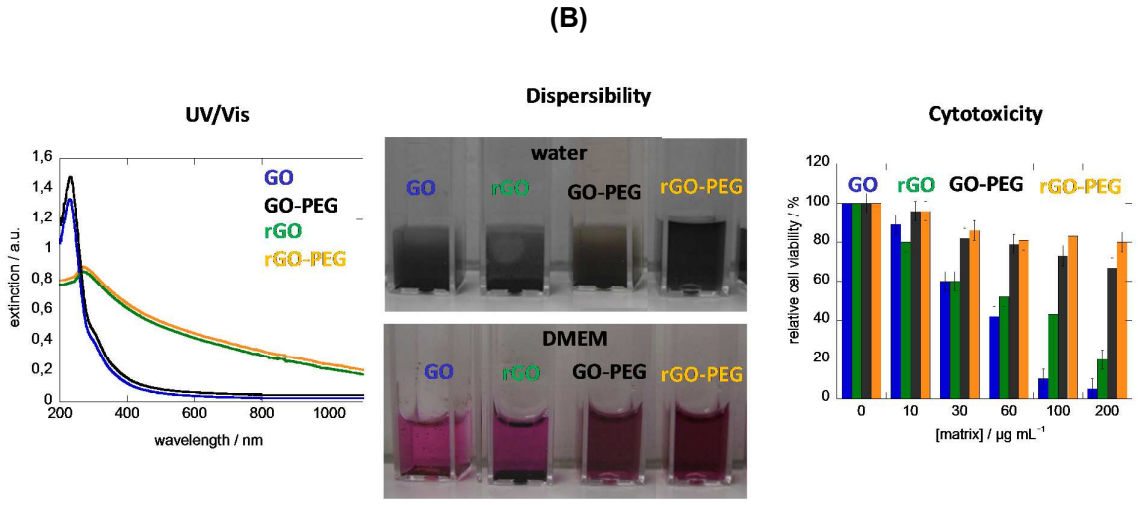

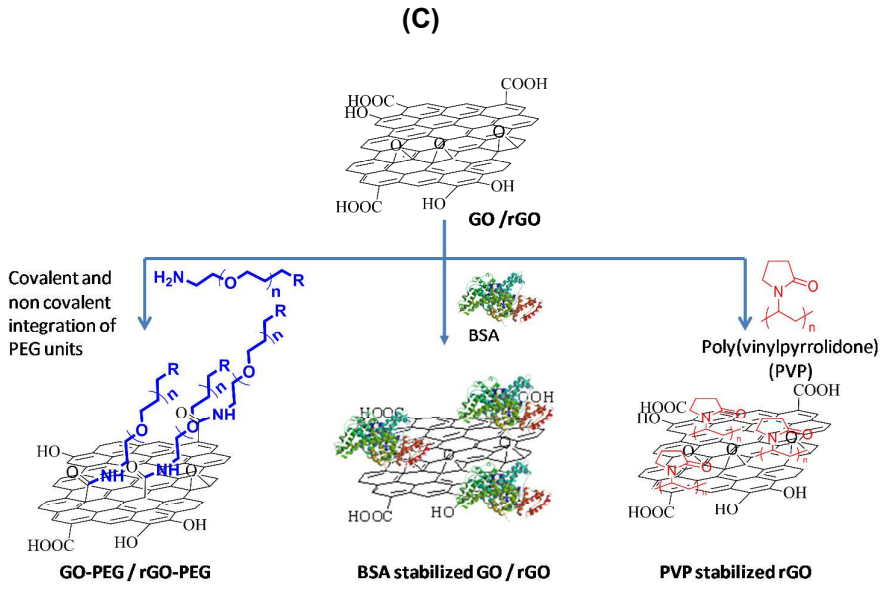

Figure 3: Graphene oxide and reduced graphene oxide: (A) their formation, (B) UV-vis absorption characteristics, water and cell medium dispersibility (60 µg mL^{-1}), and relative cell viability of HeLa cells upon incubation with different concentration of GO, rGO, GO-PEG and rGO-PEG for 72 h, (C) Different concepts for the formation of water dispersible GO and rGO.[24, 31 35, 36]

3. Preparation of rGO and its properties

The reduced form of GO, reduced graphene oxide (rGO), can provide GO with enhanced and modified optical and electrical properties and has garnered a lot of research interests. Reduction of GO to rGO can be achieved chemically (e.g. hydrazine monohydrate, sodium borohydride, hydroquinone), thermally, photochemically and other means.[28, 37-52] Hydrazine monohydrate is still most widely used, mainly due to its strong reduction activity to eliminate most oxygen-containing functional groups of GO and its ability to yield stable rGO aqueous dispersions.[50] However, with hydrazine as the reducing agent, its residual trace may strongly decrease the performance of rGO-based devices. In addition, hydrazine is a highly toxic and potentially explosive chemical. To avoid using hydrazine, many environmentally friendly and high-efficiency reductants have been developed and used for the reduction of GO, including vitamin C,[53, 54] amino acid,[54] reducing sugar,[52] alcohols,[44] hydroiodic acid,[55] reducing metal powder,[56, 57] sodium citrate,[58], tea,[59] lysozyme,[60] dopamine,[48, 61] etc. Compared to GO, rGO showed enhanced absorption over a wide wavelength window (**Figure 3B**), making it particularly appealing for photothermal applications. While rGO is often less cytotoxic than GO (**Figure 3B**), the cytotoxicity of rGO depends strongly on its preparation and the degree

of reduction (residual oxygen-containing groups).[62-65] However, as rGO tends to aggregate strongly due to π–π stacking interactions, chemical modifications of rGO has become indispensable which will in turn affect the cytotoxicity of rGO (**Figure 3B**). We have recently compared PEG-modified GO and PEG-modified rGO and found that PEF-rGO is somehow less cytotoxic than GO-PEG.[66] This observation was believed to be partially due to the difference in shape: GO-PEG displays a needle-like morphology, while rGO-PEG has a spherical shape. This example illustrates the difficulty to pin down a priori the expected cytotoxicity of these materials where size, shape, solubility as well as surface functions are all dictating the overall cell viability.

4. Fabrication of graphene/Au nanoparticles

The principal driving force for the growing research trends in the field of graphene-metal nanohybrids is the formation of nanocomposite materials of superior properties, resulting from the combination of the properties of GO and graphene with metal NPs. GO and graphene have a number of properties which make them more favorable materials compared to other carbon-based materials such as carbon nanotubes (CNTs), the most studied carbon-based nanomaterial, for the synthesis of nanocomposite structures.[67] There are currently two synthetic routes for the preparation of graphene-Au NPs composite materials. The dispersion of Au NPs on GO or rGO sheets provides an easy way to decorate graphene sheets with Au nanostructures. Encapsulation of Au clusters inside graphene-based cages is the other approach (**Figure 4**).

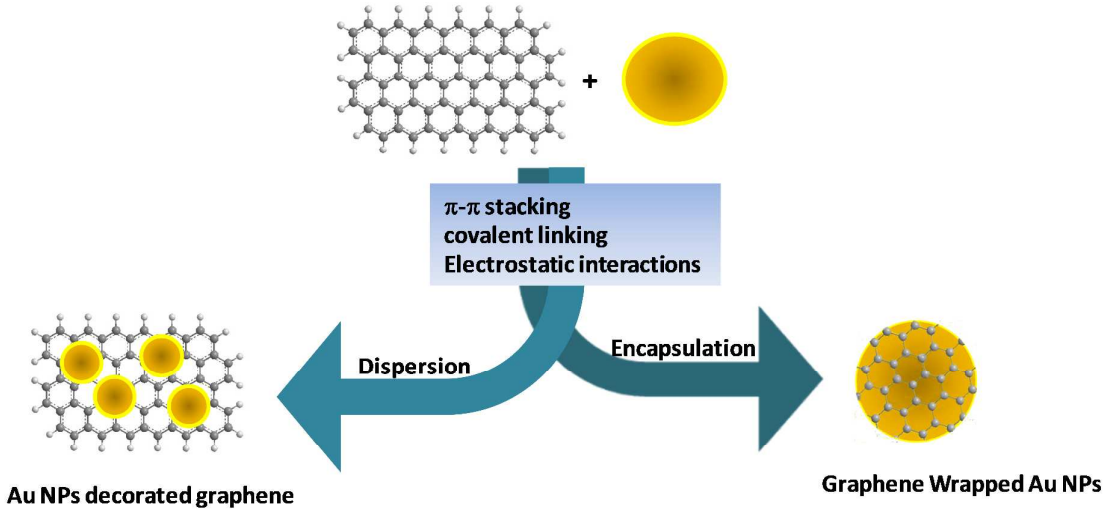

Figure 4. Decoration of GO and rGO with Au nanostructures using different interaction forces.

GO and rGO are considered adapted for both approaches, as their oxygen-containing functional groups are essential for further chemical reactions and integration of Au NSs through electrostatic interactions, covalent linkage and π-π stacking (**Figure 4**). Big attention is currently dedicated to the *in situ* synthesis of different Au NSs on rGO or GO nanosheets, among which are stars, rods, clusters,[68] nanowires,[69] nanocubes.[70] Next to the local formation of catalytic sites in Au NSs decorated graphene, which can be used for the development of high performance biosensors, catalytic and energy storage devices, an important feature of the integration of Au NSs onto GO or rGO sheets is the inhibition of aggregation of the resulting graphene sheets in dry state and in solution. Although single layer sheets of GO can be isolated, the van der Waals interactions of individual GOsheets are so strong that aggregation of graphene sheets occurs with the tendency to form graphite layered structure. The presence of metal NPs on graphene oxide (GO) sheets prevents restacking of the graphene sheets.[71] Motivated by this finding, recent research efforts have focused on the synthesis of metal NPs- GO/ (rGO composite materials. The Au NSs are acting as a spacer, increasing the distance between the graphene sheets, thereby making both faces of graphene accessible.

4.1. Au NSs embedded graphene nanocomposites

Synthesis of Au NSs loaded graphene nanocomposites can be broadly classified into two categories viz. *in situ* and *ex-situ* growth. In the *in situ* approach, simultaneous chemical reduction of GO and Au salt is carried out in order to synthesize Au NPs-rGO composite materials while the *ex situ* approach involves the synthesis of Au NPs of desired size and shape and their transfer onto graphene, GO or rGO matrix.

4.1.1. *Ex situ*

Graphene oxide and reduced graphene oxide

In the *ex-situ* method, the Au NPs are synthesized separately from GO or rGO nanosheets and are linked by utilizing electrostatic, *π-π* or van der Waals interactions for binding. In this respect, 2-mercaptopyridine modified Au NPs are linked to GO nanosheets using *π-π* stacking (**Figure 5A**).[69] The use of cysteine as linker molecule is in particular attractive. As it contains both thiol and amino groups, linking to the carboxylic acid groups of GO via its NH_2 group and to Au NRs via SH group can be achieved. The integrated Au NRs were found to separate the GO sheets within 3D layer-by-layer structure. Extensive 3D tomography study revealed that graphene sheets are placed in parallel manner rather than in random one. [69] Poly(N-vinyl-2-pyrrolidone) (PVP) was proposed by Hu et al. as stabilizing surfactant to

prevent the aggregation of GO sheets, to which Au NRs were loaded (**Figure 5B**).[36] They also noticed a significant change in the plasmonic behavior of the GO-Au NRs matrix with a red shift from 780 to 830 nm of the transversal plasmonic mode.[36] GO nanosheets functionalized with (3-mercaptopropyl)triethoxysilane (MPTES) were synthesized to improve the affinity for Au NPs.[72] Using a self-assembled method, the MPTES-functionalized GO was dispersed in DMF under ultrasonication for 5 h and then reduced with hydrazine at 95°C for 1 h. Finally, Au NPs with well-defined size (2-5 nm) were added to the reduced graphene solution.

The main advantage of this approach is the good control over the particle size, shape and loading. Spherical[31, 69, 73-75] and rod shaped Au NSs were used for the decoration of GO.[76, 77] The driving force is considered to be electrostatic interaction between negatively charged GO and positively charged CTAB- or cysteine-functionalized Au NRs. Moreover, the method was preferably used for the decoration of GO rather than rGO; the latter can be easily obtained through *in situ* reduction processes. A general platform for the assembly of Au NSs onto GO and rGO was developed by Deng and co-workers.[35] Bovine serum albumin (BSA) was used as both reducing agent and stabilizer to prepare BSA-GO/rGO-Au NPs composites according to **Figure 5C**.

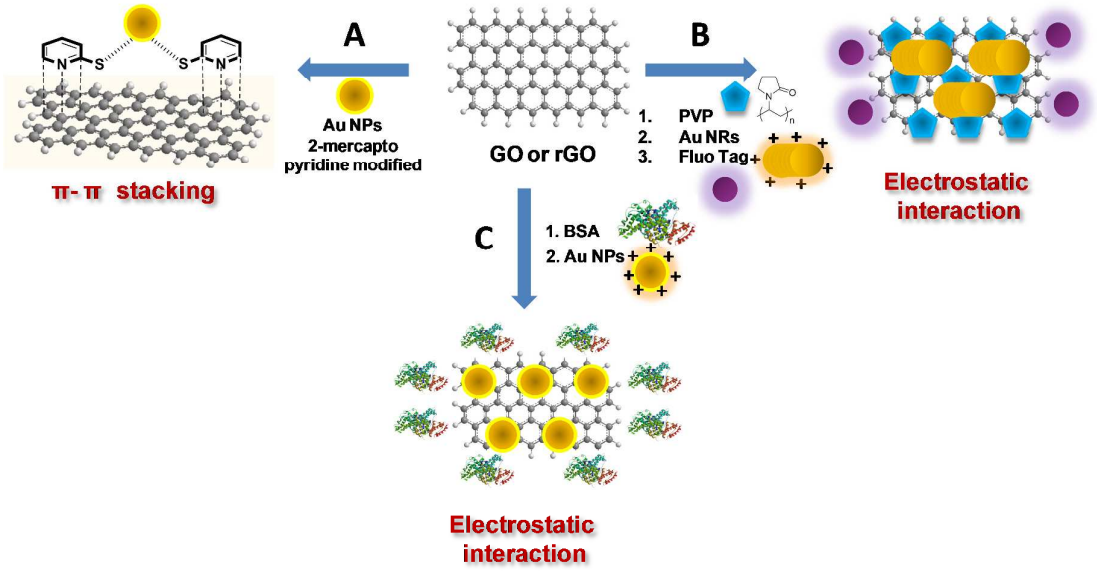

Figure 5. *Ex situ* approaches for the integration of Au NSs onto GO and rGO: (A) *π-π* stacking interaction of 2-mercaptopyridine modified Au NPs with GO nanosheets (Reprinted with permission from Huang et al., Nanoscale, 2010, 2, 2733-2738); (B) Poly(N-vinyl-2-pyrrolidone) (PVP) modified GO and loading of Au NRs by charge interaction (Reprinted with permission from Hu et al., Carbon, 2013, 51, 255); (C) Bovine serum albumin (BSA) as

stabilizing and reducing agent for GO with subsequent Au NPs integration (Reprinted with permission from Liu et al., JACS, 2010, 132, 7279).

Graphene

Next to GO and rGO, graphene thin films can also be decorated with Au NSs by thermal evaporation of Au via lithographic approaches. It has been found that Au deposited by thermal evaporation on graphene interacts differently with this substrate depending on the layer number of graphene sheets (**Figure 6A**). With the aim to explore the capacity of graphene to probe surface enhanced Raman (SERS) activity, Au NPs of well-defined dimensions (140, 210 or 320 nm) were deposited onto a multilayer system composed of a Si/SiO_2 (300 nm)/graphene system (**Figure 6B**) through thermal evaporation using masks.[78] Significant Raman enhancements (up to 35) could be measured for both G and 2D bands which scaled with the nanoparticles cross section [78] and the number of graphene layers.[79] We have shown lately that gold nanoarrays can be directly transferred onto graphene thin film using e-beam lithography (**Figure 6C**).[80]

(A)

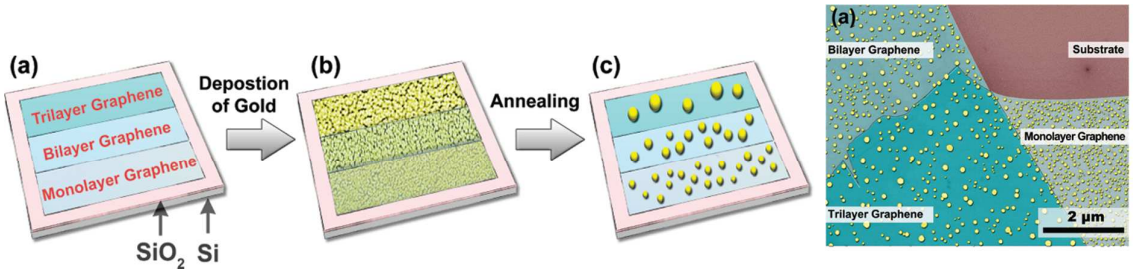

(B)

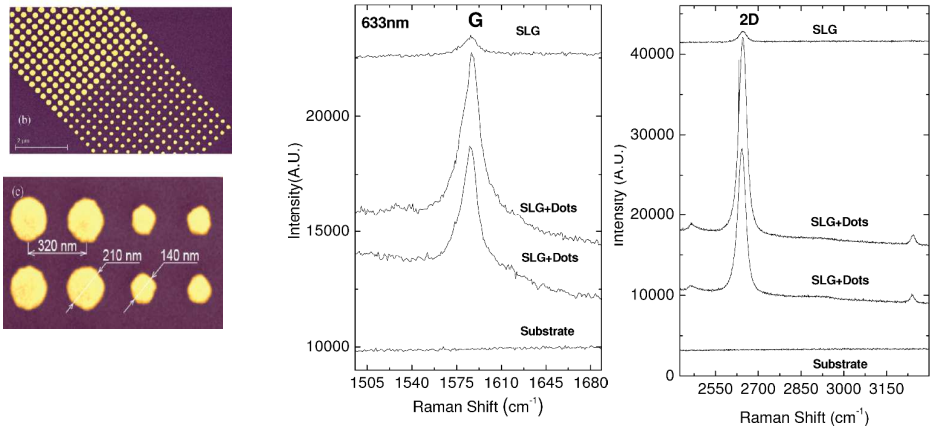

(C)

(a) (b) (c)

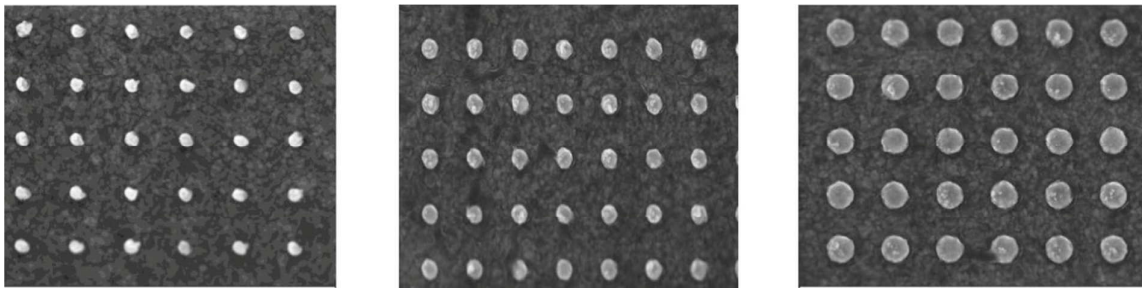

Figure 6: Decoration of graphene with ordered array of Au NPs: (A) Influence of the number of graphene layers on the morphology of the deposited nanostructures after annealing at 1260°C in vacuum for 30 s (Reprinted with permission from Zhou et al., JACS, 2010, 132, 944) ; (B) SEM image of Au NPs modified graphene sheets (SiO_2 (purple), graphene (blue), gold electrodes and dots (yellow)) and Raman spectra (laser wavelength of 633 nm) (Reprinted with permission from Schedin et al., ACS Nano, 2010, 4, 5617); (C) SEM images of graphene-coated gold thin films decorated with Au NPs by EBL with center-to-center distance of 300 nm. The particles are 50 nm in height and 80 nm (a), 110 nm (b), and 140 nm (c) in diameter (Reprinted with permission from Maurer et al., Plamonics, 2014, 9, 507).

4.1.2. *In situ synthesis of Au NPs on GO and rGO*

While the *ex-situ* approach is well adapted to form controlled GO-, rGO- and graphene-Au NSs nanocomposites, most work done in this field focused on *in situ* approaches.[69, 72, 81-84]

Reduction processes in mixed solution

In most cases, a GO suspension is mixed with $HAuCl_4$ and the mixture is treated with a reducing agent such as sodium borohydride, sodium citrate, hydrazine hydrate, ascorbic acid, glucose, etc., resulting in simultaneous reduction of Au^{3+} solution to Au^0 and GO to rGO (**Figure 7A**).[82] Although the mechanism of reduction is not clearly understood, involvements of three steps are hypothesized: the oxygen functionalities of GO provide the reactive nucleation sites. After reduction of Au cations by the reducing agent such as citrate,[58, 85, 86] sodium borohydride,[70, 87, 88] ascorbic acid,[89-91] tyrosine,[92] poly(diallyldimethylammonium chloride) (PDDA),[93] sodium dodecyl sulfate(SDS),[94] ionic liquid,[95] as well as sonolysis,[83, 96] the growth of Au particles starts; the nanoparticles remain attached to the GO sheet. The reduction agents used simultaneously reduce GO to rGO, resulting in the formation of Au NPs-rGO nanocomposites. While so far it is impossible to distinguish the role of each oxygen containing group on the nucleation of Au NPs, oxygen-rich GO platforms are reported to promote Au NPs integration.[70] As a proof, thermally reduced GO, hydrazine reduced GO and

conventional GO were used in a study to estimate the influence of level of reduction on the nucleation growth.[82] Scanning electron microscopy (SEM) analysis of obtained Au/graphene composites revealed the absence of Au NPs in case of hydrazine reduced GO, a homogeneous distribution of discrete Au NPs on the surface of GO and agglomerated Au NPs with a scarce distribution on the surface of thermally heated GO (**Figure 7B**). Song et al.[97] reported that GO surfaces enriched with carboxylic acid groups did not facilitate Au seeding, while thiol-functionalized GO[97, 98] possesses high affinity to gold allocating the seeds in a highly ordered manner. Yang et al. used the ethanethiol-perylene tetracarboxylic diimide (ETPTCDI)-mediated strategy for the preparation of highly ordered Au NPs on rGO nanosheets in a two-step process (**Figure 7B**).[99] The perylene moiety strongly binds to GO, while the thiol functionalities of ETPTCDI allocate Au seeds. Subsequent reduction with hydrazine in the presence of ammonia gave the corresponding rGO-ETPTCDI. Thereafter, the $HAuCl_4$ precursor is added to the reaction mixture and Au nanodots are formed without the addition of any reducing agent. Electron transfer from rGO-ETPTCDI is believed to be the cause for the reduction of Au^{3+} to Au^0. Furthermore, to avoid particles' aggregation mercaptoacetic acid was added during the formation of the Au particles.

Au NPs-rGO composites could be also synthesized using sodium citrate as environmentally friendly reducing and stabilizing agent.[58] In this one pot synthesis, citrate ions act as a capping agent for the simultaneous reduction of the Au ions and GO. Au NPs of ~7 nm in size were uniformly distributed over the rGO nanosheets. A green i*n situ* approach for the synthesis of aqueous stable rGO-Au NP hybrids using PVP as a stabilizer and ascorbic acid as reducing gents for both GO and gold ions was proposed by Iliut et al. more recently.[100] Muszynsky *et al.* have applied a solution-based process to synthesize Au NPs of 3-30 nm in diameter supported on octadecylamine modified GO, making them readily dispersible in tetrahydrofuran.[88] Recently, Gkikas et al reported on the simultaneous formation and stabilization of gold nanoparticles on GO covalently modified with poly(L-proline) (PLP).[101]

The *in situ* growth of Au NPs on the surface of poly(diallyldimethylammonium chloride) (PDDA) modified GO using $NaBH_4$ as reducing agent improved the dispersion of the Au NPs, but also stabilized cholinesterase with high activity and loading efficiency.[102] The formation of Au NPs/rGrO nanohybrid was confirmed by XRD (**Figure 7C**). GO shows a characteristic peak at 2θ = 10.4°, while rGO has a characteristic peak at 2θ = 27.7°. Such a peak is also observed in the XRD pattern of Au NPs-rGO nanocomposite. The XRD pattern revealed that the Au NPs are crystalline with a face-centered cubic packing arrangement of bulk metal.

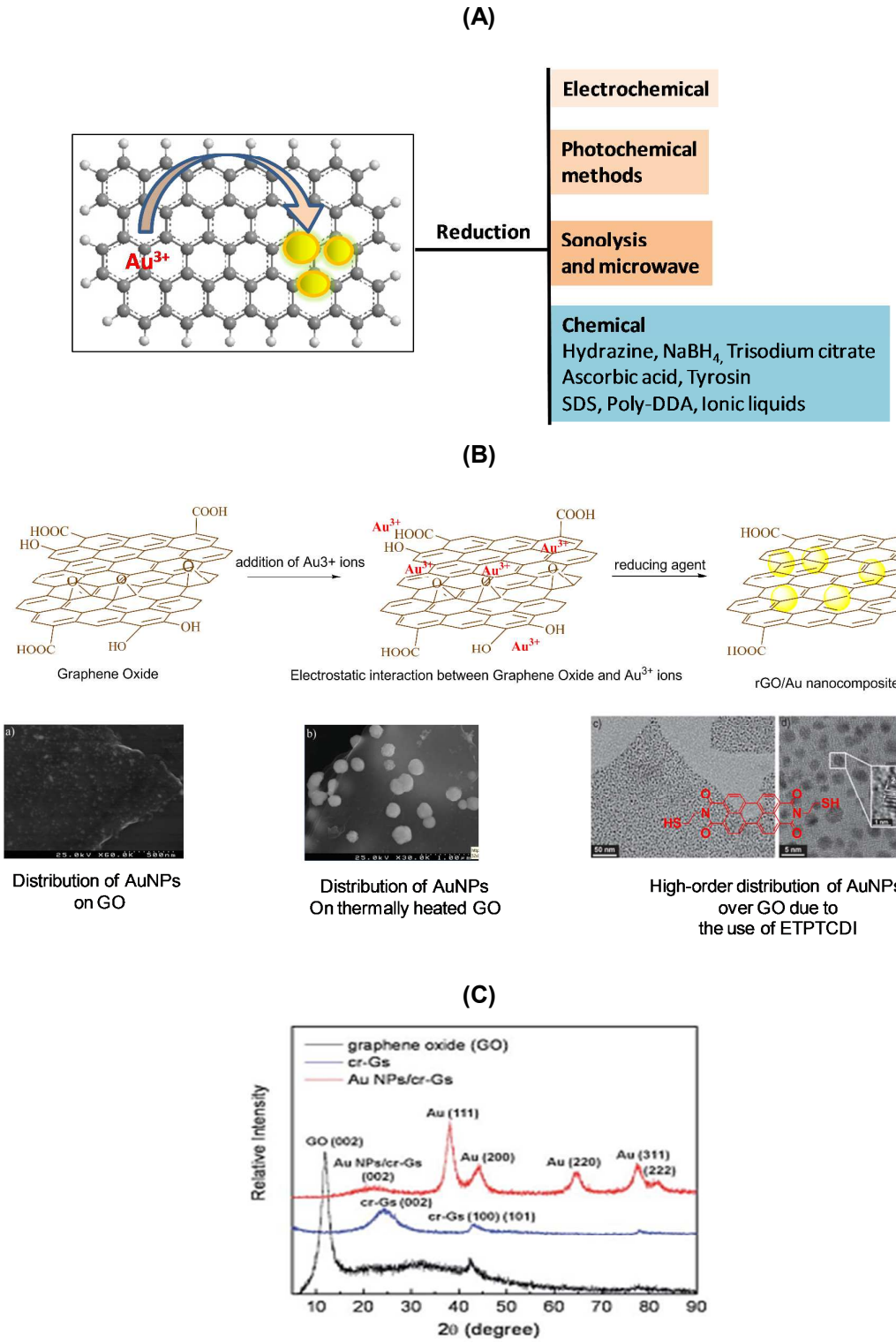

Figure 7. (A) Different *in situ* reduction strategies; (B) Influence of chemical state of GO on the distribution of Au NPs: SEM and TEM images (Reprinted with permission from Goncalves et al., Chem. Mater., 2009, 21, 4796 and Yang et al., Adv. Mater., 2012, 24,

1864);[99] (C) XRD pattern of GO, rGO and Au NPs/rGO nanohybrid. (Reproduced with permission from Y. Wang, et al., J. Mat. Chem. 2011, 21, 14, 5319).

Alternative processes

Next to the formation of Au NSs/graphene nanocomposites during reduction processes in mixed solution, the direct reduction of Au ions on rGO was reported.[103] rGO thin films, prepared by GO reduction with hydrazine, were deposited by vacuum filtering a solution of rGO suspension on quartz and immersed in an aqueous solution of $HAuCl_4.3H_2O$. During the immersion process, Au NPs were produced by spontaneous reduction of Au^{3+} on the rGO sheets. The mechanism of reduction of Au^{3+} ions on rGO involves galvanic displacement and redox reaction by relative potential difference. It is believed that Au NPs deposition was promoted by electrons present on the negatively charged rGO. This was further supported by the negative zeta potential value (- 39 mV) measured on the rGO aqueous suspension at pH 7, and the reduction potential of +0.38 V *vs* SHE estimated from ultraviolet photoelectron spectroscopy (UPS). This value is much lower than +1.002 V *vs* SHE corresponding to the reduction potential of $AuCl_4^-$, suggesting a spontaneous reduction of Au^{3+} ions on rGO.

Electrochemical deposition is an efficient and green technique for the synthesis of Au NPs–rGO nanocomposites, produced by simultaneous electrochemical reduction and electrodeposition of Au NPs onto rGO.[104, 105] Fu *et al.* synthesized Au NPs-rGO nanocomposites by electrochemical co-reduction of Au salt and GO in ionic liquid.[105]

Photochemical and photothermal methods are other green approaches investigated for the synthesis of Au NPs-GO composite materials to avoid the commonly used toxic chemicals. Moussa *et al.* investigated the reduction Au metal ions using 532 nm laser and tungsten lamp irradiation of a mixture of GO and metal ions derived from $HAuCl_4$ in different solvents such as water-ethanol, water-polyethylene glycol (PEG) or pure water.[106] Ethanol and PEG act as scavengers for the holes, generated upon irradiation of GO, and thus promote GO reduction by the photogenerated electrons. In the reducing environment, provided by ethanol or PEG, the photogenerated electrons reduce the metal ions, and since the alcohol radicals (C_2H_4OH) are strong reducing agents they undergo oxidation to CH_3CHO and therefore reduce GO to rGO.[106]

High-frequency ultrasound reduction is a convenient and clean approach to carry out the synthesis of Au NPs-graphene nanocomposites. The interaction between ultrasound and gas molecules (monoatomic or diatomic), in aqueous solutions, results in the growth and violent collapse of microbubbles. This collapse generates high temperature conditions within the bubbles, which leads to the formation of highly reactive $H^{\cdot}$ and $OH^{\cdot}$ ions. In general, the $H^{\cdot}$

radicals rapidly recombine or react with H_2O, which rules out its possibility to act as reducing agent for other substrate. If the organic solutes are volatile, the reducing radicals are directly generated within the bubbles. These radicals can reduce the substrate such as metal ions in solution, GO to rGO or a mixture of metal ions-GO. Vinodgopal *et al.*[83] reported on the ultrasound-induced reduction of GO and $HAuCl_4$ in 2% aqueous solution of poly(ethylene glycol) to synthesize Au NPs-rGO nanocomposites.

Formation of anisotropic gold nanostructures on rGO

The *in-situ* synthesis is also adapted for the formation of rGO matrices modified with anisotropic Au NPs. The roughness of GO seems to be the underlying driving force. The formation of Au snow flake particles different from multipod and star shaped Au NSs is governed only by the presence of GO (**Figure 8A**).[107] Marzan and co-workers showed clearly the influence of GO on the morphology of branched Au NSs.[108] The Au NSs formed in the absence of GO displayed thinner and more abundant branches when compared to rGO-Au NSs prepared by the same protocol (**Figure 8B**). By simply varying the ratio of $[Au^{3+}]/[Au^{seeds}]$ concentration, different morphologies were obtained. Nanopatches of GO anchored Au NSs were successfully synthesized using HEPES (4-(2-hydroxyethyl)-1-piperazineethanesulfonic acid) mediated route.[109] HEPES also facilitates anisotropic growth and shape control of Au NSs along the (111) direction through strong affinity of the piperazine ring for the (110) planes of Au in comparison to weak adsorption on the (111) planes. HEPES reduction of Au precursors occurs due to oxidation of N atom of a piperazine ring and usually proceeds at room temperature and neutral pH. In this work, the important role of GO concentration was shown. By increasing the GO to Au ratio, enhanced nucleation and high anisotropy occurred. This indicates the role of GO for controlled growth of near-infrared (NIR) tunable Au NSs (**Figure 8C**).

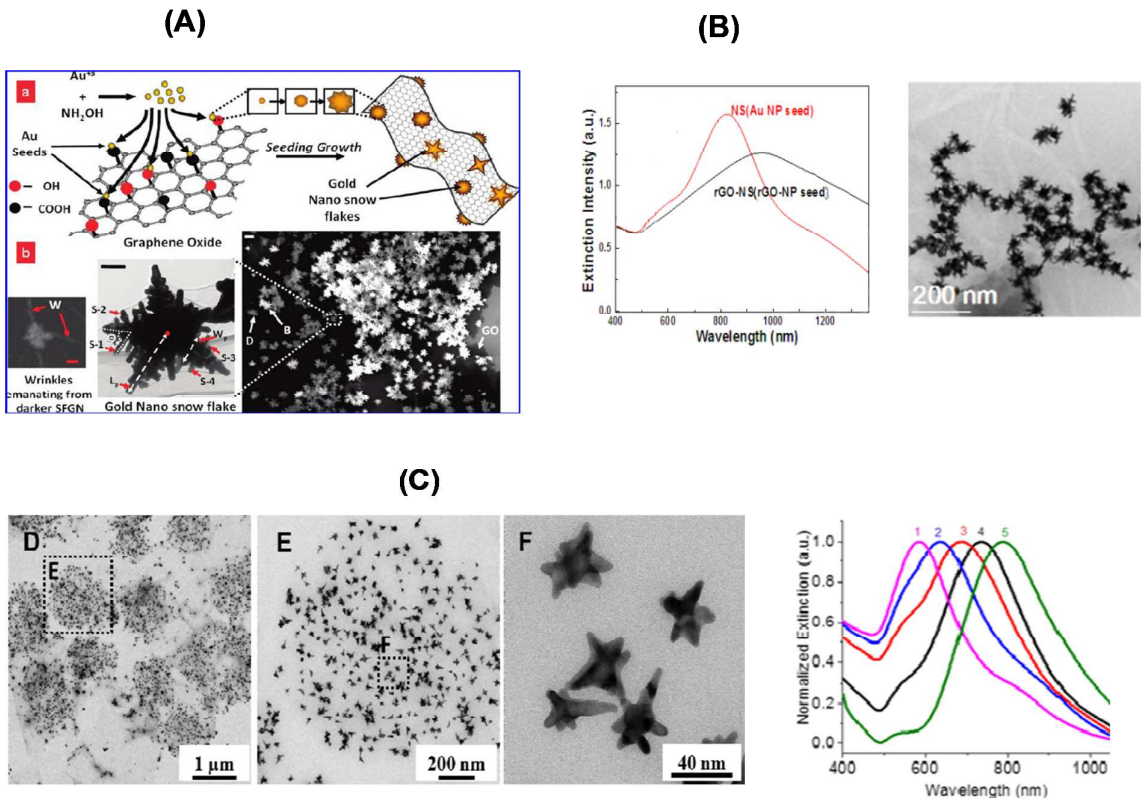

Figure 8: (A) Hydroxylamine mediated anisotropic growth of gold nano snowflakes on GO substrate (Reprinted with permission from Goncalves et al., Chem. Mater., 2009, 21, 4796); (B) The decoration of rGO with gold nanostars by Ag^{+} mediated protocol, (Reprinted with permission from Wang et al. ACS Applied Materials & Interfaces **2014,** 6, (24), 21798-21805); (C) TEM and UV/Vis images of HEPES mediated GO anchored Au NSs nanopatches synthesis (Reprinted with permission from Nergiz et al. ACS Appl. Mater. Interfaces 2014**,** 6, (18), 16395-16402).

4.2 Graphene oxide and reduced graphene oxide wrapped Au NPs

As discussed briefly beforehand, the usefulness of GO and rGO for nanoparticles formulation is limited by their poor colloidal stability, which necessitates surface chemistry modification with stabilizing agents. The fabrication of a continuous shell of graphene, GO or rGO over Au NPs is proposed to overcome such limitation. The presence of oxygen functionalities on GO and rGO results in an overall negative zeta potential of such nanostructures, facilitating the interaction with positively charged Au NPs, like those formed though stabilization with CTAB. One of the first attempts to fabricate graphene-like carbon shells around Au NPs was that proposed by Chopra et al.[18] Au NPs on 3-mercaptopropyltrimethoxysilane (MPTMS) modified

Si substrates were used as catalysts for the growth of the graphene shell using a CVD process (**Figure 9A**). Carbon shells of ~1.2-2.8 nm in thickness were formed over a period of 1 h, corresponding to ~5-9 independent graphene layers with an interplanar spacing of 0.34 ± 0.01 nm. CVD growth times above 4 h caused the rupture of the graphene shell and dissociation from the Au NPs. A modified approach was recently reported by Bian et al. [110] An aqueous solution of $HAuCl_4$, used as the metal precursor, was loaded onto fumed silica powder and subjected to methane CVD for graphene shell growth. Modified with polyoxyethylene stearyl ether molecules made the formed graphene-coated gold nanostructures water dispersible and extremely stable under extreme pH environments and high salt conditions (**Figure 9B**).[110]

Next to CVD approaches, chemical strategies have shown in addition to allow the wrapping of GO and rGO over Au NSs.[27, 111-113] Kohane and co-workers developed plasmonic nanoparticles coated with rGO through electrostatic interactions between nanosized GO and cysteamine stabilized Au NPs or CTAB stabilized Au NRs, followed by chemical reduction to generate partially reduced GO.[111] As measured by high resolution-transmittance electron microscopy (HR-TEM), rGO shells of ≈ 1 nm (Au NPs) and 2.5 nm (Au NRs) were formed in this way (**Figure 9C**). Raman analysis showed distinctive Raman peaks at 1355 cm^{-1} (D band) and 1593 cm^{-1} (G band) together with bands at 2710 cm^{-1} (2D band) and 2900 cm^{-1} (D+D' band) indicative of the successful chemical reduction of GO layers. The obtained nanostructures had an overall negative surface potential and showed improved colloidal stability compared to rGO nanosheets. A similar approach was used by Xu et al. to prepare GO wrapped Au NRs.[112] A different approach to produce individually GO wrapped Au NPs was reported by Ma et al.[114] The nanostructures were fabricated in a one-step synthetic method by mixing $HAuCl_4$ with nanoscale GO sheets and adding $NaBH_4$ at certain time intervales (**Figure 9D**).

(A) **(B)**

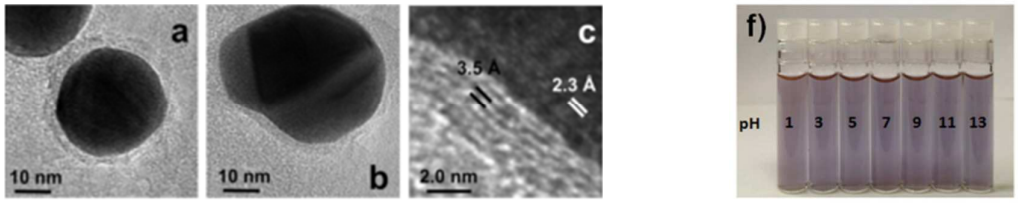

(C)

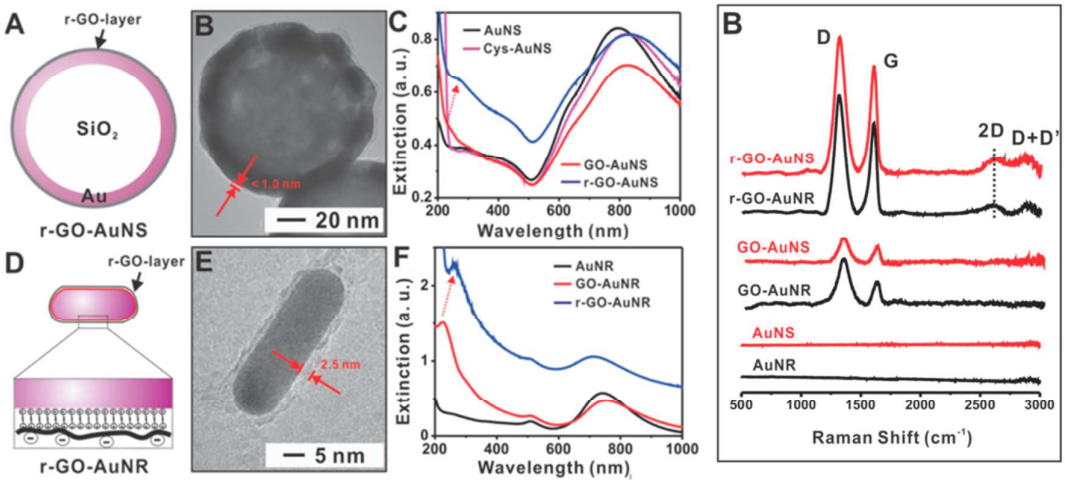

(D)

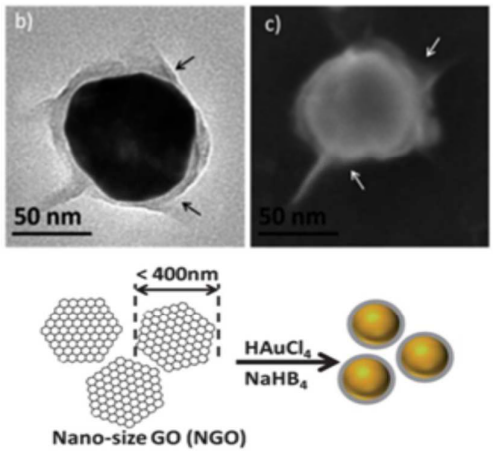

Figure 9: (A) TEM images of CVD based synthesis of graphene wrapped Au NPs (Reprinted with permission from Chopra et al. *Chem. Mater.* **2009,** 21, 1176); (B) Stability of different graphene wrapped Au NPs suspensions (Reprinted with permission from Bian et al. *Sci. Rep.* **2014,** 4, 6093); (C) TEM images of rGO-Au NRs and rGO-Au NSs together with optical and Raman images, (Reprinted with permission from Lim et al. *Nano Lett.* **2013,** 13, 4075); (D) TEM images of 20 nm Au-GO capsules (Reprinted with permission from Ma et al. *J. Mater. Chem. B* **2013,** 1, (47), 6495).

We have shown lately the interest of covalently linking rGO to Au NRs. Such a hybrid can be synthesized *via* amide bond formation between amine-PEG-terminated rGO (rGO-PEG-NH_2) and HOOC-PEG-Au NRs, formed following the well established seed-mediated procedure in

the presence of CTAB and dicarboxylic polyethyleneglycol in the growth solution (**Figure 10**).[115, 116] A representative TEM image of the rGO-PEG-Au NRs hybrid shows the presence of a rGO-PEG layer of ≈ 1.5 nm around the Au NRs. The UV-vis spectrum of the rGO-PEG-Au NRs hybrid displays two bands at 589 nm and 680 nm corresponding to the transverse and longitudinal plasmon oscillations of the Au NRs, respectively (**Figure 10B**). The presence of rGO is furthermore evidenced by the absorption maximum at 270 nm and an overall increase in the absorption from the visible to the NIR. The rGO-PEG-Au NRs hybrid (average size of 60±15 nm) is in addition highly dispersible in aqueous media and stable for several months (**Figure 10C**). In contrast to the HOOC-PEG-Au NRs, the *in vitro* toxicity of the rGO-PEG-Au NRs hybrid to MDA- MB-231 cells was drastically improved (**Figure 10D**). No obvious decrease of cell viability was noticed for MDA- MB-23 cells when incubated with rGO-PEG-Au NRs (10 µg ml^{-1}) for 78 h in strong contrast to Au NRs, where at the same concentration cell viability was around 20 %. The hybrid also proved to be less toxic than GO, but somewhat more cytotoxicity than rGO-PEG-NH_2.

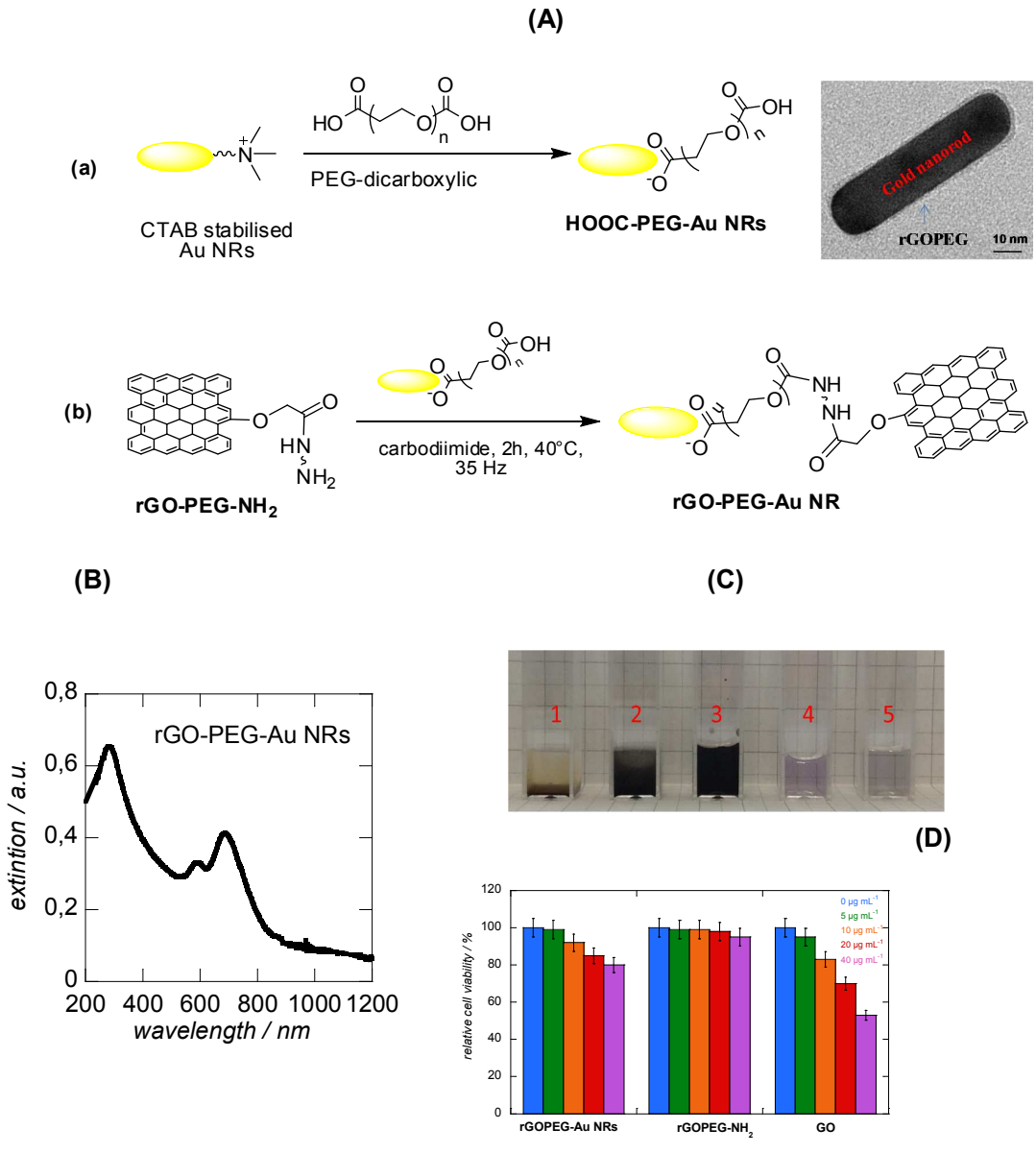

Figure 10. (A) (a) Synthesis of HOOC-PEG-Au NRs, (b) covalent linking of rGO-PEG-NH_2 with HOOC-PEG-Au NRs; TEM image of a Au NR coated with rGO-PEG-NH_2; (B) UV-vis of rGO-PEG-Au NRs; (C) Stability of different matrices in PBS (100 µg/ml): (1) GO, (2) rGO-COOH, (3) rGO-PEG-NH_2, (4) Au NRs, (5) rGO-PEG-Au NRs; (D) Relative cell viability of MDA MB 231 cells upon incubation with different concentrations (0-40 µg mL^{-1}) of rGO-PEG-Au NRs, rGOPEG-NH_2 and GO for 78h.[27]

4.3 Graphene-wrapped Au NPs

While not extensively investigated, some examples on the wrapping of surface linked Au NPs with graphene sheets have been reported lately (**Figure 11**).[117-119] Such approaches were in particular expected to improve the SERS signals.[120, 121] Hegg et al. post-coated Au NSs with graphene sheets to form Au cavities.[118] As seen in **Figure 11A**, the structures consisted of two Au disks with a height of 45 nm and a diameter of ≈100 nm with an interparticle distance of ≈30 nm on a flat SiO_2 surface of 300 nm in thickness. Graphene, prepared by mechanical cleavage,[122] was transferred on top of the structures. Suspended in this way graphene is under tensile strain and possesses enhanced Raman signal compared to unperturbed graphene, with Raman enhancement of up to 10^3 fold.[118] Wang et al. reported on the formation of graphene coated Au nanopyramide tips.[119] **Figure 11B** illustrates a typical sample that consists of three regions located immediately next to each other: the Au tipped surface, the flat Au surface and the surface of flat SiO_2 of 200 nm in thickness. The hexagonally ordered Au nanopyramide arrays of ≈250 nm base with radius of curvature at the apex as small as 1 nm are fabricated on a continuous Au film of 200 nm in thickness using the nano-casting process described by Sun et al.[123] It is based on the self-assembly of polystyrene beads on silicon substrates followed by plasma etching and Au deposition. Graphene transfer over the formed Au tips was achieved by mechanical transfer of CVD grown graphene (**Figure 11B**). Interestingly, such structures showed a giant enhancement of graphene Raman signals of up to 10^7.[119]

(A) **(B)**

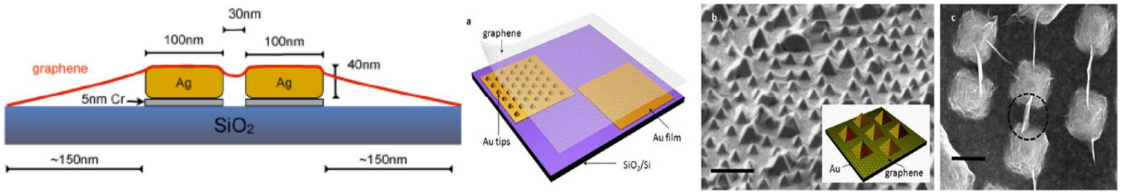

Figure 11. (A) Sketch of the gold cavities sample configuration (Reprinted with permission from Heeg et al., Nano Lett., 2013, 13, 301); (B) Schematics of graphene-Au nanopyramid sample and SEM image of graphene on Au tips (scale bar 1 μm, inset: schematic image of graphene on Au tips) and of hexagonally arranged arrays of Au tips which sharply folded graphene (scale bar 200 nm). The dotted black circle indicates a hanging graphene fold between neighboring tips (Reprinted with permission from Wang et al., ACS Nano, 2012, 6, 6244).

5. Applications of gold-graphene nanocomposites

Since the successful fabrication of single layered graphene, graphene and its derivatives have been the shining stars in materials science. More recently, the use of graphene in biomedicine has aroused widespread interest for various applications including drug and gene delivery, cancer therapies, biomedical imaging, biosensors as well as tissue engineering scaffolds. The first report on the use of graphene as therapeutic dates back to the work of Dai et al. in 2008, where pegylated graphene oxide (PEG-GO) was used for the delivery of water insoluble cancer drugs.[24] The drug-loaded PEG-GO was tested for cancer cell killing capability and exhibited high potency with IC_{50} values of 6 nM for the human colon cancer cell line HCT-116. This work illustrated the potential of graphene-based nanocarrier as an efficient drug-delivery agent for aromatic and water insoluble drugs. The exciting achievements over the last years have been extensively reviewed by different researchers and will not be further discussed here.[124, 125] Instead, a brief overview of recent work on biomedical applications of Au-graphene nanocomposites will be discussed (**Figure 12**), as these composite materials opened up different exciting therapies and applications for biology.

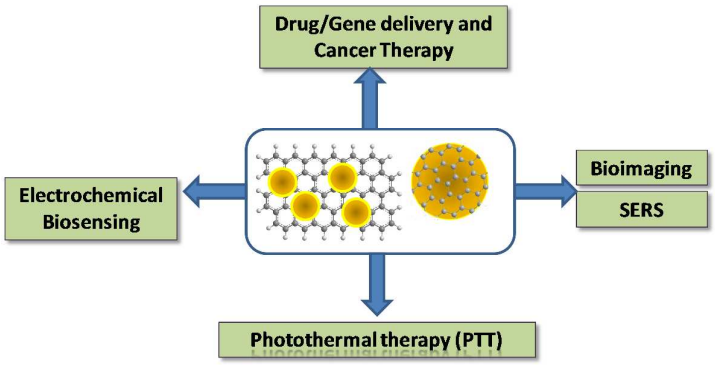

Figure 12: Biomedical applications of Au-graphene nanocomposites.

5.1. Drug/gene delivery and cancer therapy

GO is an ideal nanocarrier for water insoluble drugs and gene delivery. The unique structure features such as high surface specific area (2630 m^2/g), large and planar sp^2-hybridized carbon domains and the presence of a large number of oxygen-containing groups, render GO stable in physiological media and capable of loading of drugs *via* chemical conjugation or $\pi-\pi$ stacking interactions. For example, doxorubicin (DOX) loading of 6.05 mg/mg at 0.32 mg/mL drug concentration was achieved on GO.[75]

Xu et al. combined chemo- and photothermal (see **section 5.2**) targeted therapy by designing hyaluronic acid modified Au NRs/GO core shell nanocomposites loaded with DOX for the selective treatment of hepatoma Huh-7 cancer cells (**Figure 13**A).[112] Around 15.3% of DOX was released from the nanostructures at pH=5.3, while by means of NIR irradiation release of up to 34.5% was achieved. The chemo-photothermal combined therapy showed 4-fold higher targeted cell death rates than single chemotherapy or photothermal therapy. In line with this work, graphene-isolated Au nanocrystals (GIAN) modified with DOX provided an efficient therapeutic platform for combined chemo- and photothermal targeted therapy. Obvious differences in cell deaths were observed for DOX loaded GIAN with and without NIR (808 nm) treatment giving rise to photothermally-enhanced chemotherapeutic effect.[110] Polyethyleneimine (PEI) modified GO encapsulated Au NSs were recently proposed as novel gene vector for pDNA (**Figure 13B**). The efficiency of the Au NSs-GO-PEI hybrids was shown to be high (65%). Moreover, viability of HeLa cells was preserved (90%) compared to poor cell survival using PEI as gene vector.[126] Yuan et al investigated recently the effect of multifunctional micro-RNA-122 loaded GO@Au nanocomposite on drug-resistant liver cancer cells.[127] Indeed, it is now well known that the expression of micro-RNA-122 is down-regulated in many hepatoma cells. The development of a combination of monoclonal P-glycroprotein antibodies, folic acid and micro-RNA-122 loaded GO@Au nanocomposites showed to promote drug-resistant HepG2 cell apoptosis with drug targeting and controlled release propert. [127]

(A)

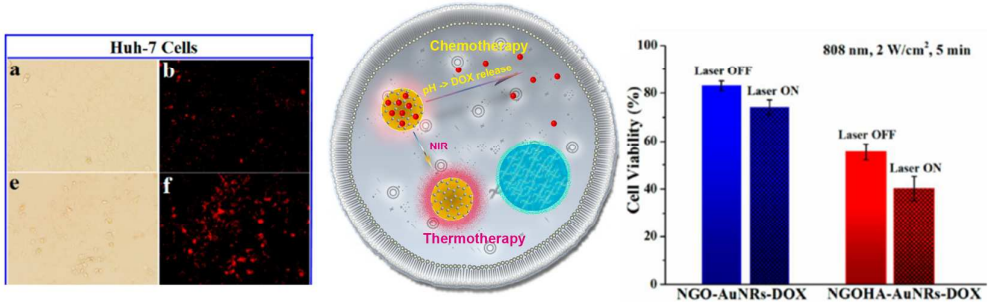

(B)

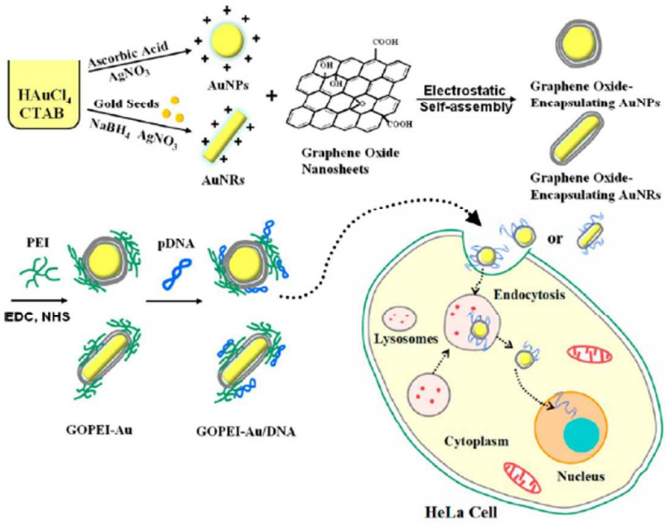

Figure 13. (A) Hyaluronic acid modified Au NRs/GO core shell nanocomposites loaded with doxorubicin for the selective treatment of hepatoma Huh-7 cancer cells (reprint with permission for Xu et al., ACS Appl. Mater. Interfaces 2013, 5, 12911-12920); (B) Schematic illustration of the synthesis of GO-PEI-AuNPs and GO-PEI-AuNRs, and the possible mechanism of gene delivery (reprint with permission for Xu et al., ACS Appl. Mater. Interfaces 2013, 5, 2715-2724).

5.2. Photothermal Therapy (PTT)

While the high surface area is primordial for efficient drug and gene loading, the strong optical absorption in the near infrared light (NIR) region makes GO (rGO)-based nanocomposites in addition suitable for photothermal therapy (PTT). [128] One of the current modalities for PTT is the use of NIR light absorbing agents that convert optical energy into heat, leading to the thermal ablation of cancer cells and pathogens. The use of NIR has the advantage that water, melanin and hemoglobin have absorption minima in this region and light between 700-900 nm is most likely to pass directly through tissues without significant absorption and heat generation.[129] The high photothermal effect under low power NIR irradiation of GO and in particular rGO due to their effective light-to-heat conversion has made graphene-based materials competitive photothermal agents.[66, 94, 130-133] Although rGO shows a 6-fold great NIR absorbance than GO,[134] the low quantum efficiency of rGO and its broad absorption spectrum renders it less sensitive to specific wavelengths. To overcome this limitation and to enhance the photothermal effect, Au-graphene hybrid cargos have been proposed. Indeed, Au-based nanomaterials exhibit strong visible to NIR absorption owing to

the localized surface plasmon resonance effects, rendering them the most power agents for PTT cancer treatment and bacteria killing.[8, 135, 136] Different Au-graphene hybrid materials have been proposed in the last years and have shown enhanced therapeutic efficiency at physiologically safe doses.[68, 110, 112, 114, 137] El-Shall and co-workers demonstrated the coupling of photothermal effects of gold nanostructures of controlled size and shape with GO nanosheets dispersed in water.[138] It was noted, that laser irradiation of gold nanorods in the presencee of GO resulted in well-dispersed ultrasmall gold nanoparticles of 2.9±1.7 nm in diameter when illuminated for 10 min at 532 nm (4 W). [138] The enhanced photothermal effect of Au nanostructures coated with rGO in the NIR was first investigated by Kohane and co-workers.[111] When stimulated by NIR light, Au nanoshells and Au nanorods coated with rGO produced enhanced photothermal effects (**Figure 14A**).[111] The effectiveness of these nanomaterials for PTT was demonstrated with cultured human umbilical vein denotherlila cells (HUVECs). While in the absence of irradiation HUVECs exposed to rGO coated Au particles showed no significant cytotoxicity (**Figure 14Ac)**, under irradiation (3 W/cm^2, 808 nm) a time-depended decrease in cell viability was observed. The photothermal therapeutic response of cancer cells to aptamer-modified gold nanoparticles embedded on GO was recently shown to facilitate targeted treatment of tumor cells by NIR light-activatable photothermal therapy.[139] Due to the specific interaction between the MUC1-binding aptamer and the MUC1 transmembrane mucin glycoprotein on the cell membrane selective targeting is achieved. Furthermore, under NIR illumination the nanocomposites induced transient increase in the expression of heat shock proteins (HSP70), which may cause irreversible damage to cancer cells. [139]

More recently, graphene wrapped Au NRs were used for the photothermal ablation of bacteria.[27, 140] The development of non antibiotic based treatments against bacterial infections is a complex task. New strategies to treat such infections are thus urgently needed. We developed lately Au NRs coated with rGO-PEG (rGO-PEG-Au NRs) for the selective killing of uropathogenic *E. coli* UTI89 (**Figure 14B**). Targeted killing of *E. coli* UTI89 was in addition achieved though functionalization of the photothermal target with multimeric heptyl α-D-mannoside probes. This currently offers a unique biocompatible method for the ablation of pathogens with the opening of probably a new possibility for clinical treatments of patients with urinary infections.

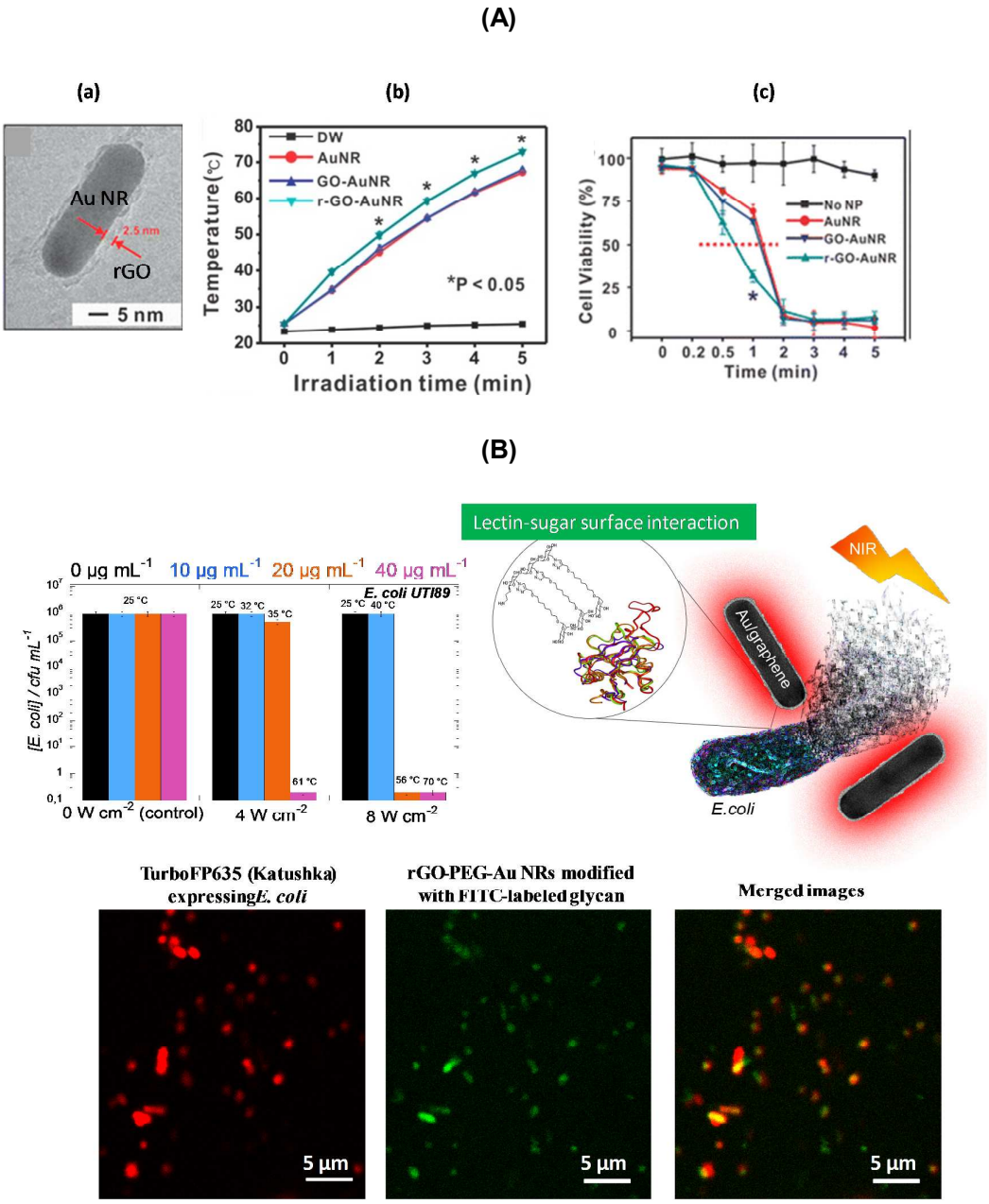

Figure 14. Chemo-photothermal therapy with graphene wrapped Au NSs: (A) TEM image of graphene wrapped Au NR (a), heating curves (b) and cell viability under light illumination (reprint with permission from D.-K. Lim et al. Nano Lett., 2013, 13, 4075-4079.); (B) Change of *E. coli UTI89* concentration in the presence of multimeric heptyl-α-D-mannoside modified rGO-PEG-Au NRs particles upon irradiation at 4 or 8 W cm^{-2} for 10 min at 700 nm together with effective targeting demonstration. The fluorescent images correspond to *E. coli* UTI89 expressing the fluorescent Katuschka protein, to FTIC-labeled multimeric heptyl-α-D-mannoside modified rGO-PEG-Au NRS and the overlap of both images (with permission from Ref. K. Turcheniuk et al. J. Mater. Chem. B, 2015, 3, 375).

5.3. Biosensing and Bioimaging

5.3.1 Electrochemical sensors based on gold nanoparticles-graphene hybrids

Graphene and its derivatives have been intensively used for the detection of diverse biomolecules including dopamine, amino acids, biomolecules, etc.[22, 141-144] Several types of biosensors have been constructed including fluorescence energy transfer (FRET), plasmonic, matrix-assisted laser desorption/ionization time-of-flight mass spectrometry (MALDI-TOF MS), field-effect transistor (FET) and electrochemical means. One field where Au NPs/graphene nanocomposites have had an enormous impact is in electrochemical-based sensing. Carbon materials are widely used in both analytical and industrial electrochemistry, as they show a wide potential window and are low cost materials in comparison to metal electrodes such as Au or Pt. In the case of graphene-based electrodes, next to a large potential window, fast heterogeneous electron transfer kinetics for various analytes and the involvement of additional "chemical amplification effects" (e.g. in the case of aromatic structures such a dopamine interacting strongly with rGO *via* π–π stacking interactions)[145] have made these electrodes well adapted for sensing. The integration of Au NPs into graphene nanosheets allows in certain cases to efficiently improve the sensitivity and detection limit of the sensor due to improvement of the electron transfer or through its catalytic reaction with certain analytes (e.gh. hydrogen peroxide) (**Table 1**). The synergetic effect of rGO matrix decorated with Au NPs on the electrochemical performance of a glucose sensor was for example shown by Shan et al.[146] Immobilization of glucose oxidase onto rGO-Au NPs-chitosan matrices resulted in a composite electrode with a detection limit of 180 μM for glucose and a linear range from 2 to 14 mM.

The concept of using Au NPs decorated graphene for the catalysis of electrochemical reactions has been used to detect hydrogen peroxide (**Figure 15**). Fang *et al.* took advantage of the cationic properties of poly(diallyldimethylammonium chloride) (PDDA) functionalized graphene for the preparation of graphene/Au NPs heterostructure with enhanced electrochemical catalytic ability towards hydrogen peroxide.[147] Indeed, the sensor exhibited a detection limit of 0.44 μM over a linear range from 0.5 μM to 0.5 mM. The good performance of the sensor was ascribed to the high loading and uniform dispersion of the Au NPs on the graphene nanosheets. We recently investigated the reducing properties of tyrosine for the *in situ* synthesis of aqueous stable rGO/Au NPs hybrids from GO and Au ions. The resulting nanocomposite showed electrochemical activity for nonenzymatic detection of H_2O_2 with a detection limit of 20 μM over a wide linear range from 0.02 to 25 mM. Jiang and co-workers used Au NP-graphene hybrid structures for the detection of H_2O_2

in living cells. The results indicated that a higher efflux of H_2O_2 is observed in tumor cells versus normal cells.[148]

DNA sensing is another common application of Au NP/graphene hybrids. Mandler and co-workers showed that the surface of graphene/Au NP electrodes can be easily modified by thiolated DNA through strong Au-S bonding.[149] When the target DNA completely hybridizes with the probe DNA, the electron is transferred from the electrode surface to methylene blue to catalyze ferrocyanide, thus showing a reduction peak in the DVP measurements. A DNA biosensor using nanocomposites of Au NPs/toluidine blue in rGO. was recently proposed by Peng et al.[150] Differential pulse voltammetry was employed to monitor the hybridization of DNA by measuring the changes in the peal current of toluidine blue. Under optimal conditions, the decreased currents were proportional to the logarithm of the concentration of the target DNA in the range of 1×10^{-11} -1×10^{-9} M with a limit of detection of 2.95×10^{-12} M. [150]

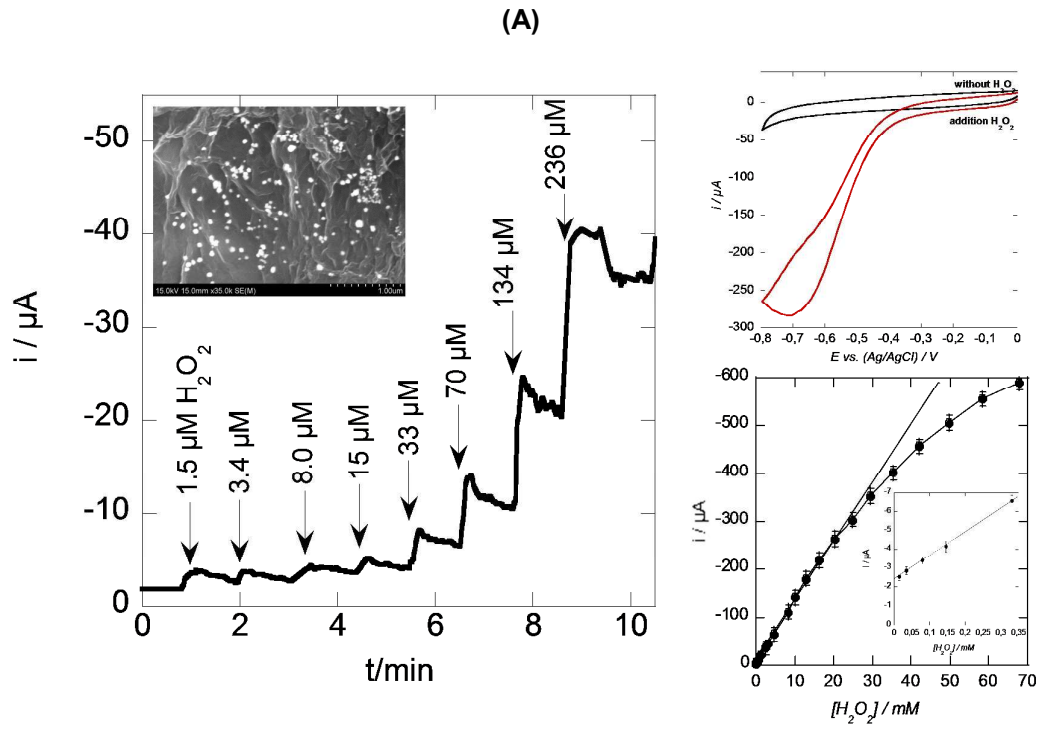

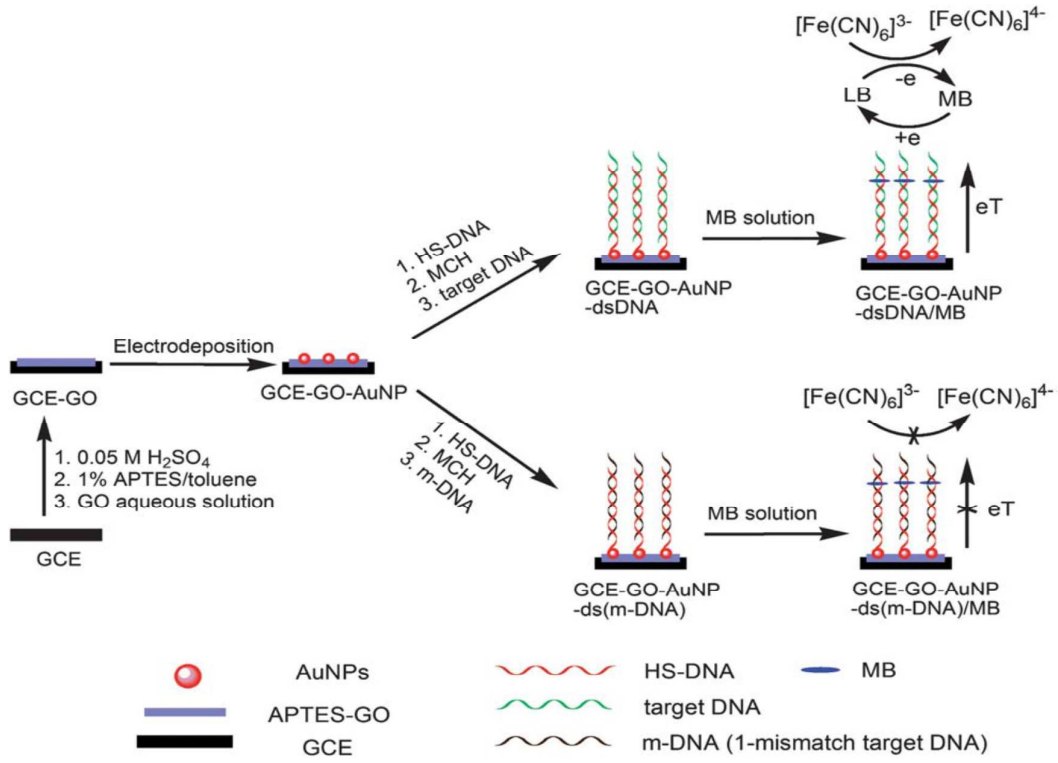

Figure 15. (A) Amperometric response curve at rGO/Au NPs/Tyr/GC polarized at -0.6 V *vs.* Ag/AgCl with subsequent additions of H_2O_2, inset : SEM image of rGO/Tyr/Au NPs nanohybrid; Cyclic voltammograms of rGO/Au NPs/Tyr/GC in N_2-saturated 0.1 M PBS solution (pH 7.4) in the absence and presence of 10 mM H_2O_2 scan rate: 50 mV/s together with calibration curve.[151] ; (B) Schematic illustration of an electrochemical DNA sensor (reprint permission from Ref. Wang et al., Nanoscale, 2012, 4, 2728-2733).

Table 1: graphene/Au NPs hybrid based electrodes for electrochemical sensing applications

hybrid	**analyte**	**LOD** **linear range** **sensitivity**	**Ref**
rGO-Au NPs-chitosan/GODx	glucose	LOD=180 μM 2-14 mM 99.5 μA μM^{-1} cm^{-2}	146
Graphene:MWCNT-Au NPs	glucose	4.8 μM 5-175 μM 29.72 μA μM^{-1} cm^{-2}	152
GO-Ag/Au NPs-mercaptophenylboronic acid	glucose	0.33 mM 2-6 mM	153
Nitrogen-doped graphene quantum dots/au NPs	Hydrogen peroxide	0.12 μM	154

PDDA-Au NPs/graphene	uric acid	0.1 μM 0.5-20 μM 103.8 μA μM^{-1} cm^{-2}	155
rGO/Au NPs/enzyme	cholesterol	0.05 μM 0.05-0.35 mM 3.14 μA μM^{-1} cm^{-2}	156
Graphene-Au NPs	L-histidine	0.1pM 10pM-10 μM	157
rGO/Au NPs	L-lactate tumor biomarker	0.13 μM 10μM-5 mM 154 μA/mM cm^2	158
Single-layered GO-Au NPs	DNA	100 fM	149
Graphene-Au NPs/PANI	DNA	2.11 pM 10-1000 pM	159
rGO-Au NPs/toluidine blue	DNA	2.95 pM 0.1 pM-1 nM	150
PDDA-modified rGO-Au NPs	angiogenin	0.064 pM 0.1 pM-5 nM	160
rGO-Au NPs/anti-CEA	antigen Carcinoembryonic	0.01 ng mL^{-1} 0.05-350 ng mL^{-1}	161
Graphene-Au-Fe_3O_4	prostate specific antigen	5 ng mL^{-1} 0.01-10 ng mL^{-1}	162
rGO-Au NRs-antibody	transferrin	0.0375-40 μg mL^{-1}	163
rGO/Au@Pd/thionine/HRP/Ab2	Carbohydrate antigen 19-9	006 U mL^{-1} 0.015-150 U mL^{-1}	164
Graphene-aptamer-Au NPs	ATP/Hg^{2+}	ATP: 15 nM (10 nM-4 mM) Hg^{2+}: 0.5 nM (0.5-500 nM)	165
rGO-Au NPs	cells	5.2×10^3 cells mL^{-1} 1.6×10^4-1.6×10^7 cells mL^{-1}	166

PDDA: poly(diallyldimethyl ammonium chloride); HRP: horseradish peroxidase

Next to electrochemical sensing, a graphene-gold NPs hybrid FET sensor for the detection of proteins was proposed by Chen et al.[167] Thermally reduced graphene oxide sheets were decorated with Au NPs which were covalently conjugated to anti-immunoglobulin G (IgG) antibodies. Upon introduction of the target protein, the direct current was measured resulting in a detection limit of 13 pM, among the best reported for carbon-based materials. The sensors showed also excellent selectively when exposed to other protein mismatches.

5.3.2 Gold nanoparticles-graphene hybrids for surface-enhanced Raman spectroscopy (SERS)

Surface-enhanced Raman scattering (SERS), a spectroscopic technique combining modern laser spectroscopy with the optical properties of metallic nanostructures, provides one of the most effective ways to dramatically enhance the Raman signal of molecules attached to nanometer-sized metal structures.[168] Consequently, SERS has been widely applied in different fields, including sensing and medical diagnosis.[168, 169] It was used for the detection of single molecule interaction,[170] and identification of biomolecules,[171-173] genes,[174] proteins,[175] cancer cells,[148, 176] and others.[177, 178 179]

Traditionally, Au and Ag NPs are used for SERS studies.[180] Anisotropic structures such as Au NRs have in this respect proved to be highly efficient SERS substrates.[108] Recent studies have demonstrated that graphene and its derivatives have the ability to enhance Raman signals as do Au NSs.[181] The discovery of graphene-mediated SERS (G-SERS or simple GERS) by Ling et al.[181] began with an accidental experiment, in which it was found that there are many "emerging bands" of mechanically exfoliated graphene when it is treated with organic solvents. Systematic G-SERS experiments using dyes such as phthalocyanine as Raman probes clearly showed that graphene enhances the Raman signals of the molecules (**Figure 16A**). Strictly speaking, graphene does not fit the traditional definition of a SERS substrate because of the absence of the electromagnetic field contribution found in other plasmonic materials such as metal nanostructures. The origin of GERS is chemical enhancement. This leads to the conclusion that the GERS enhancement should be highly relevant to the chemical nature of graphene. Indeed, it was shown that GO possesses higher enhancement factor than just graphene sheet.[182] From the discussion above, it can be expected that the combination of graphene and Au NPs will result in a dual-enhancement of the Raman signal *via* chemical (graphene) and electromagnetic (Au NPs) enhancement.[69 107, 183, 184] Hu et al. compared recently the Raman signals of adsorbed aromatic dye molecules such as crystal violet onto GO, Au NRs and Au NRs/graphene hybrids (**Figure 16B**) and validated clearly the enhanced SERS signal of Au NRs/GO nanohybrids.[185]

(A)

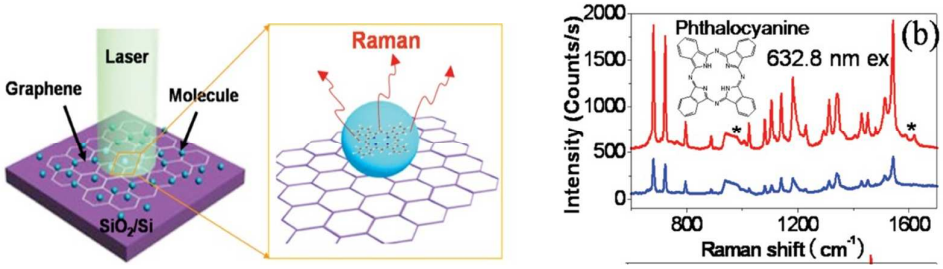

(B)

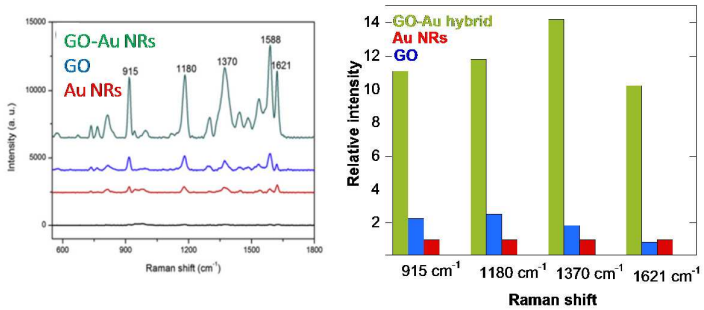

Figure 16: (A) The G-SERS effect: (a) Schematic illustration of the molecules of graphene deposited on Si/SiO_2 (300 nm). (b) Comparison of the Raman signals of phthalocyanine (0.2 nm in thickness) deposited on graphene (red line) and on Si/SiO_2 substrate (blue) upon 632.8 nm excitation (Reprinted with permission from Ling et al., Nano Lett. 2010, 10, 553) ; (B) Raman spectra of Crystal Violet on Au NRs (red), GO (blue), GO-Au NRs (green) surfaces together with relative intensity of the observed Raman signals (Reprinted from the permission Hu et al. Carbon, 51, 2013, 255).

Au NPs/graphene hybrid structures have also shown their potential for molecular bioimaging. HeLa cells incubated with GO/Au NPs hybrids exhibit a much stronger Raman signal than that recorded on cells incubated with pristine GO (**Figure 17A**).[186] Guo et al. reported around the same time on a one-pot green route for intracellular synthesis of gold nanostructures assisted by poly(vinylpyrrolidone) (PVP) functionalized GO.[187] The distribution of the nanostructures in cells allowed for the sensitive monitoring of intracellular chemical compositions including the cytoplasm, nucleoplasm, and even the nuclei using SERS (**Figure 17B**).[187] The group by Zhang et al used SERS to study the mechanism of the cellular uptake of GO@Au NPs nanocomposites.[188] An inhomogeneous distribution of GO inside the cell was seen and with internalization into Ca Ski cells mainly *via* clathrin-mediated endocytosis. [188]

More recently, Raman mapping of the graphitic band of GO of GO-Au NPs revealed that the hybrid was concentrated in the cytoplasm of the cell with weak or no signal from the nucleus (**Figure 17C**). Kim and co-workers moved towards the detection of neural stem cell differentiation using 3D GO encapsulated Au NPs (**Figure 17D**).[179] The Raman peaks achieved from undifferentiated stem cells on the hybrid were 3.5 times higher than peaks obtained from normal metal structures and were clearly distinguishable from those of differentiated cells. The number of C=C bonds and the Raman intensity at 1656 cm^{-1} were found to correlate positively. Indeed, the membrane of undifferentiated cell line is rich in unsaturated molecules possessing C=C bonds being the feature to differentiate cells by SERS.[179]

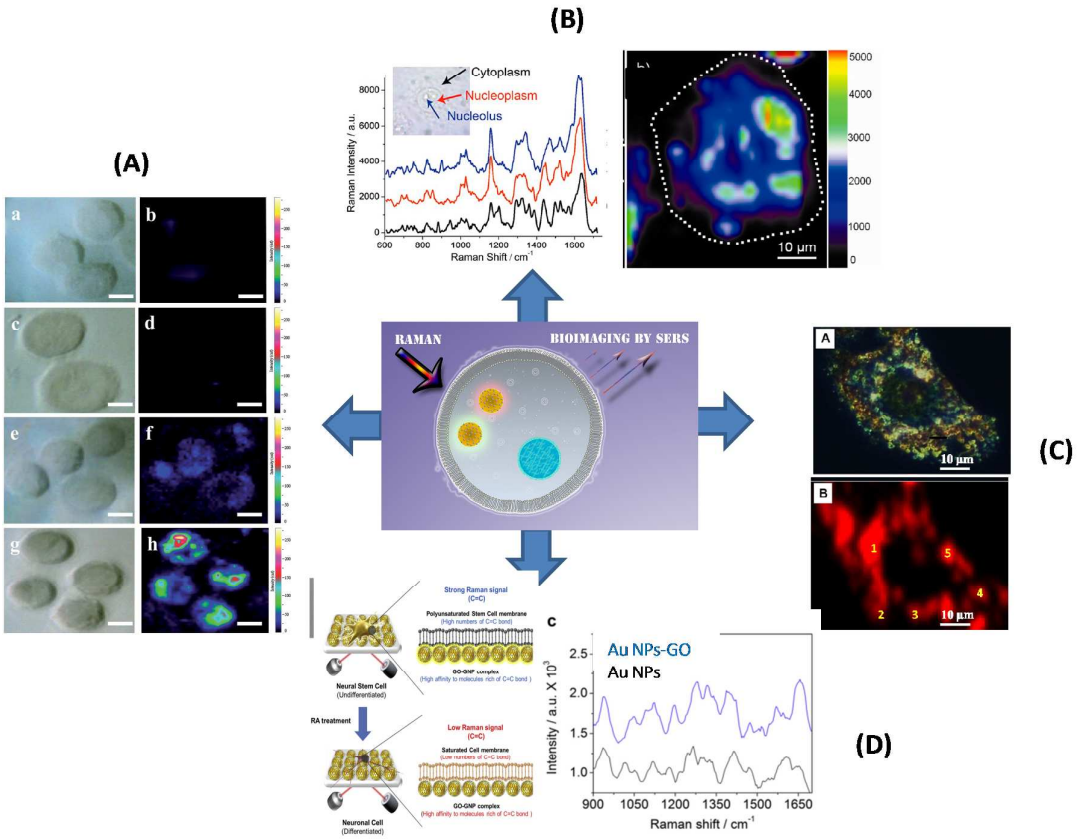

Figure 17: Raman bioimaging using Au NPs/graphene hybrids: (A) Optical (a, c, e, g) and Raman (b, d, f, h) images of Hela 229 cells. Cells were incubated with GO (e, f) and Au NPs/GO hybrids (g, h) at 37 °C for 24 h before imaging. Cells incubated in medium without GO (a and b) and in medium with Au NPs (c and d) are shown as control (scale bar: 10 mm) (reprint with permission from Ref. Liu et al., Nanoscale, 2012, 4, 7084-7089); (B) GO/PVP/IGAuNs SERS spectra of A549 cells collected from the regions corresponding to the cytoplasm, nucleoplasm, and nucleolus (upper) together with typical SERS images of A549 cells contained with GO/PVP/IGAuNs, showing the distribution of Au NSs inside the cell. The dotted lines in the images are drawn to indicate the boundaries of selected cells (reprint with permission from Ref. Liu et al., Anal. Chem. 2012, 84, 10338-10344); (C) Dark field scattering images and Raman map of G band (1600 cm^{-1}) intensity of SKBR-3 cells incubated with GO-Au NSs clearly showing the presence of GO in the cytosol and absence of the same in the nucleus (Reprinted with permission from Nergiz et al., ACS Appl. Mater. Interfaces, 2014, 6, 16395-16402); (D) Detection strategy to monitor differentiation of neuronal stem cells and Raman spectra of neuronal stem cells on Au NPs and GO/Au NPs substrates, Raman peaks obtained from previous spectra on Au (black) and GO/Au NPs (red) substrates (Reprinted with permission from Kim et al,. Biomaterials, 2013, 34, 8660-8670).

6. Conclusion and Perspectives

The development of gold-graphene nanocomposites has seen a significant progress in the last years. Within the field of electrochemical sensing, the graphene-Au NPs hybrid materials have received a significant amount of attention and improved considerably the sensitivity and selectivity that is better than graphene or Au NPs alone. Graphene- graphene-Au NPs hybrid materials showed high sensing performance to biological relevant analysts such as DNA and proteins, as well as to small molecules such as dopamine and hydrogen peroxide. The report on the fabrication of a non-enzyamtic hydrogen peroxide sensor for the sensitive detection of H_2O_2 levels in human serum and when released from human cervical cancer cells is one of the advancements in this field.[154] These developments would not have been possible without a large input from material scientists on the development of synthetic methods for decorating graphene with Au nanostructures. Although conventional CVD graphene with Au NPs showed distinctive performance in electronics and for surface-enhanced Raman imaging, the high costs involved and the low production yield made CVD graphene not the primary choice for biomedical applications. Solution phase fabricated graphene oxide (reduced graphene oxide) has thus been the material of choice for such applications. The use of such structures for photothermal therapy has been particularly attractive with real therapeutic potential. Most recently, the delivery of zinc phtalocyanine photosensitizer by means of Au@GO NPs was shown.[189] The sequential action of photodynamic therapy and photothermal therapy considerably enhanced the therapeutic effect on the treatment of HeLa cells.

Another still rather unexploited field is the use of such structures for combating microbial infections caused by diverse pathogens. One of the first reports in this direction is that of Hussain et al.[65] It was demonstrated that rGO-Au NPs nanocomposite prepared using an eco-friendly route shows good biocompatibility with cervix carcinoma, human (HeLa) cells, and possesses high antibacterial activity against two Gram-positive bacteria (*Staphylococcus aureus* and *Bacillus subtilis*) and two Gram-negative bacteria (*Escherichia coli* and *Pseudomonous aeruginosa*). The bacterial cell death is believed to be caused by the leakage of sugars and proteins from the cell membrane in contact with the Au NPs-rGO matrix. This field is still rather unexploited even though work is ongoing in this direction.

The use of gold supported graphene nanomaterials as potential vaccine carriers and adjuvants has been lately considered by the group of Zhang et al. [190] It could be shown that GO@Au NPs decorated with ovalbumin as model antigen can efficiently stimulate RAW264.7 cells to secrete tumor necrosis factor-α (TNF-α), a mediator for cellular immune response. Such nanostructurs stimulated potent humoral and cellular immune responses against

antigens. These finding will open up the potential applications of graphene-Au NPs as cancer and viral vaccines.

The research of GO based scaffolds for cell culture is a relatively new direction that deserves further investigation in the future. The accelerated growth, differentiation and proliferation of stem cells hold great promise in tissue engineering and other biomedical fields such as regenerative medicine. The future will thus bring still lots of exciting applications.

Since the biocompatibility and cytotoxicity of such hybrids can be well tuned by using appropriate surface chemistry approaches, these nanostructures will be still a focus of interest in the coming years. However, the potential long term toxicity seems to be still a major obstacle for clinical use.

Further developments in this field require the understanding of the structural properties and interaction mechanisms between the Au NPs and graphene sheets from both theoretical and experimental aspects. Moreover, another challenge is connected with the graphene matrix. As an essential matrix of the nanocomposites, the synthesis of high quality graphene is necessary and represents an important aspect for the design and preparation of nanocomposites of controlled properties. The last challenge involves the control of the size, shape, crystallinity, and distribution of the Au NPs on graphene nanosheets. Finally, both Au NPs and GO/rGO matrices offer the possibility for the functionalization of their surfaces with different molecules of interest and thus opens new avenues for designing multifunctional nanocomposites with potential applications in various areas of research. This will be achieved through multidisciplinary efforts from chemists, materials scientists, physicists and biologists.

References

1. R. Wilson, *Chem Soc Rev.*, 2008, 37, 2028-2045.
2. K. M. Mayer and J. H. H. Hafner, *Chem. Rev.*, 2011, 111, 3828.
3. S. Szunerits and R. Boukherroub, *Chem. Commun.*, 2012, 48, 8999-9010.
4. K. M. Mayer and J. H. Hafner, *Chem. Rev.*, 2011, 111, 3828-3857.
5. J. Spadavecchia, A. Barras, J. Lyskawa, P. Woisel, W. Laure, C.-M. Pradier, R. Boukherroub and S. Szunerits, *Anal. Chem.*, 2013, 85, 3288-3296.
6. S. Szunerits, J. Spadavecchia and R. Boukherroub, *Rev. Anal. Chem.* , 2014, 33, 153-164.
7. O. Zagorodko, J. Spadavecchia, A. Yanguas Serrano, I. Larroulet, A. Pesquera, A. Zurutuza, R. Boukherroub and S. Szunerits, *Anal. Chem.* , 2014, 86, 11211-11216.
8. D. Pissuwan, C. H. Cortie, S. M. Valenzuela and M. B. Cortie, *Trends Biotechnol.*, 2010, 28, 207-213.
9. E. Boisselier and D. Astruc, *Chem. Soc. Rev.*, 2009, 38, 1759-1782.

10. D. Pissuwan, S. M. Valenzuela and M. B. Cortie, *Biotechnol. Gen. Eng. Rev.*, 2008, 25, 93-112.
11. P. Gosh, G. Han, M. De, C. K. Kim and V. M. Rotello, *Adv. Drug. Deliv. Rev.*, 2008, 60, 1307-1315.
12. D. Bechet, P. Couleaud, C. Frochot, M.-L. Viriot, F. Guillemin and M. Barberi-Heyob, *Trends Biotechnol.*, 2008, 26, 612-621.
13. C. M. Goodman, C. D. McCusker, T. Ylmaz and V. M. Rotello, *Bioconjugate Chem.*, 2004, 15, 897-900.
14. T. Niidome, M. Yamagata, Y. Okamoto, Y. Akiyama, H. Takahashi, T. Kawano, Y. Katayama and Y. Niidome, *J. Control. Release*, 2006, 114, 343-347.
15. T. S. Hauck, A. A. Ghazani and W. C. W. Chan, *Small*, 2008, 4, 153-159.
16. K. Turcheniuk, C.-H. Hage, J. Spadavecchia, L. Heliot, R. Boukherroub and S. Szunerits, *Encyclopedia of nanotechnology, (ed. Bharat Bhushan), Nano-Plasmonics section, Springer Editorial, 2014*, 2015, accepted.
17. M. Kim, K. Sohn, H. B. Na and T. Hyeon, *Nano Lett.*, 2002, 2, 1383-1387.
18. N. Chopra, L. G. Bachas and M. R. Knecht, *Chem. Mater.*, 2009, 21, 1176-1178.
19. A. K. Geim, *Science*, 2009, 324, 1530.
20. A. K. Geim and K. S. Novoselov, *Nat. Mater.*, 2007, 6, 183.
21. S. Goenka, V. Santa and S. Santa, *J. Control. Rel.*, 2014, 173, 75-88.
22. P. T. Yin, T.-H. Kim, J.-W. Choi and K.-B. Lee, *Phys. Chem. Chem. Phys.*, 2013, 15, 12785-12799.
23. K. R. Ratinac, W. J. Yang, J. J. Gooding, P. Thordarson and F. Braet, *Electroanalysis*, 2011, 23, 803.
24. Z. Liu , J. T. Robinson , X. Sun and H. Dai, *J. Am. Chem. Soc.*, 2008, 130, 10876-10877.
25. C. Chung, Y. K. Kim, D. Shin, S.-R. Ryoo, B. H. Hong and D.-H. Min, *Acc. Chem. Res.*, 2013, 46, 2211-2224.
26. K. T. Nguyen and Y. Zhao, *Nanoscale*, 2014, 6, 6245-6266.
27. K. Turcheniuk, C.-H. Hage, J. Spadavecchia, A. Y. Serrano, I. Larroulet, A. Pesquera, A. Zurutuza, M. G. Pisfil, L. Heliot, J. Boukaert, R. Boukherroub and S. Szunerits, *J. Mater. Chem. B*, 2015, 3, 375-386.
28. W. S. Hummers and J. R. E. Offerman, *J. Am. Chem. Soc.*, 1958, 80, 1339-1339.
29. N. Chatterjee, H.-J. Eom and J. Choi, *Biomaterials*, 2014, 35, 1109-1127.
30. K. Wang, J. Ruan, H. Song, J. Zhang, Y. Wo, S. J. Guo and D. X. Cui, *Nanoscale Res. Lett.*, 2011, 6, 8.
31. X. Sun, Z. Liu, K. Welsher, J. T. Robinson, A. Goodwin, S. Zaric and H. Dai, *Nano Res.*, 2008, 1, 203-212.
32. S.-Z. Zu and B.-H. Han, *J. Phys. Chem. C*, 2009, 113, 13651-13657.
33. Y. X. Xu, H. Bai, G. W. Lu, C. Li and G. Q. Shi, *J. Am. Chem. Soc.*, 2008, 130, 5856-5857.
34. H. Hu, Z. Zhao, Q. Zhou, Y. Gogotsi and J. Qiu, *Carbon*, 2011, 50, 3267-3273.
35. J. Liu, S. Fu, B. Yuan, Y. Li and Z. Deng, *J. Am. Chem. Soc*, 2010, 132, 7279-7281.
36. C.-C. Hu, J. Ron, J. Cui, Y. Yang, L. Yang, Y. Wang and Y. Liu, *Carbon*, 2013, 51, 255-264.
37. D. R. Dreyer, S. J. Park, C. W. Bielawski and R. S. Ruoff, *Chem. Soc. Rev.*, 2010, 39, 228-240.
38. O. Fellahi, M. R. Das, Y. Coffinier, S. Szunerits, T. Hadjersi, M. Maamache and R. Boukherroub, *Nanoscale*, 2011, 3, 4662-4669.
39. S. Stankovich, D. A. Dikin, R. D. Piner, K. A. Kohlhaas, A. Kleinhammes, Y. Jia, Y. Wu, S. T. Nguyen and R. S. Ruoff, *Carbon*, 2007, 45, 1558-1565.
40. H. J. Shin, K. K. Kim, A. Benayad, S. M. Yoon, H. K. Park, I. S. Jung, M. H. JIn, H. K. Jeong, J. M. Kim, J. Y. Choi and Y. H. Lee, *Adv. Funct. Mater.*, 2009, 19, 1987-1992.
41. H. Park and R. S. Ruoff, *Nat. Nanotechnol.*, 2009, 4, 217-224.
42. C. A. Amarnath, C. E. Hong, N. H. Kim, B. C. Ku, T. Kuila and J. H. Lee, *Carbon*, 2011, 49, 3497-3502.

43. I. K. Moon, J. H. Lee, R. S. Ruoff and H. Lee, *Nat. Commun.*, 2010, 73, 1.
44. D. R. Dreyer, S. Murali, Y. Zhu, R. S. Ruoff and C. W. Bielawski, *J. Mater. Chem.*, 2011, 21, 3443-3447.
45. M. J. Allen, V. C. Tung and R. B. Kaner, *Chem. Rev.*, 2010, 110, 132-145.
46. O. C. Compton, B. Jain, D. A. Dikin, A. Abouimrane, K. Amine and S. T. Nguyen, *ACS Nano*, 2011, 5, 4380-4391.
47. I. Kaminska, A. Barras, Y. Coffinier, W. Lisowski, J. Niedziolka-Jonsson, P. Woisel, J. Lyskawa, M. Opallo, A. Siriwardena, R. Boukherroub and S. Szunerits, *ACS Appl. Mater. Interfaces*, 2012, 4, 5386-5393.
48. I. Kamińska, M. R. Das, J. Niedziółka-Jönsson, P. Woisel, J. Lyskawa, M. Opallo, R. Boukherroub and S. Szunerits, *ACS Appl. Mater. Interfaces*, 2012, 4, 1016-1020.
49. I. Kaminska, M. R. Das, Y. Coffinier, J. Niedziolka-Jonsson, P. Woisel, M. Opallo, S. Szunerits and R. Boukherroub, *Chem. Commun.*, 2012, 48, 1221-1223.
50. D. Li, M. B. Mueller, S. Gilje, R. B. Kaner, G. G. Wallace and G. Gordon, *Nat. Nanotechnol.*, 2008, 3, 101-105.
51. V. C. Tung, M. J. Allen, Y. Yang and R. B. Kaner, *Nat. Nanotechnol.*, 2009, 4, 25-29.
52. C. Zhu, S. Guo, Y. Fang and S. Dong, *ACS Nano*, 2010, 4, 2429-2437.
53. M. J. Fernandez-Merino, L. Guardia, J. I. Paredes, S. Villar-Rodil, P. Solis-Fernandez, A. Martinez-Alonso and J. M. D. Tascon, *J. Phys. Chem. C*, 2010, 114, 6426-6432.
54. J. Gao, F. Liu, Y. L. Liu, N. Ma, Z. Q. Wang and X. Zhang, *Chem. Mater.*, 2010, 22, 2213-2218.
55. S. F. Pei, J. P. Zhao, J. H. Du, W. C. Ren and H. M. Cheng, *Carbon*, 2010, 48, 4466-4474.
56. Z. J. Fan, K. Wang, T. Wei, J. Yan, L. P. Song and B. Shao, *Carbon*, 2010, 48, 1686-1689.
57. Z. J. Fan, K. Wang, J. Yan, T. Wei, L. J. Zhi, J. Feng, Y. M. Ren, L. P. Song and F. Wei, *ACS Nano*, 2011, 5, 191-198.
58. Z. Zhang, H. Chen, C. Xing, M. Guo, F. Xu, X. Wang, H. J. Gruber, B. Zhang and J. Tang, *Nano Research*, 2011, 4, 599-611.
59. Y. Wang, Z. X. Shi and J. Yin, *ACS Appl. Mater. Interfaces*, 2011, 3, 1127-1133.
60. F. Yang, Y. Q. Liu, L. A. Gao and J. Sun, *J. Phys. Chem. C*, 2010, 114, 22085-22091.
61. L. Q. Xu, W. J. Yang, K.-G. Neoh, E.-T. Kang and G. D. Fu, *Macromolecules*, 2010, 43, 8336-8339.
62. Y.-K. Kim, M.-H. Kim and D.-H. Min, *Chem. Commun.*, 2011, 47, 3195-3197.
63. E. L. K. Chng and M. Pumera, *Chem. Eur. J.* , 2013, 19, 8227 – 8235.
64. L. Wu, H. S. Chu, W. S. Koh and E. P. Li, *Opt. Expr.*, 2010, 18, 14395-14400.
65. N. Hussain, A. Gogoi, R. K. Sarma, P. Sharma, A. Barras, R. Boukherroub, R. Saikia, P. Sengupta and M. R. Das, *ChemPlusChem*, 2014, 79, 1774-1784.
66. K. Tucheniuk, C.-H. Hage, L. Heliot, S. Railyan, V. Zaitsev, J. Spadavecchia, R. Boukherroub and S. Szunerits, *Nano Life*, 2014.
67. S. Bai and X. Shen, *RSC Advances*, 2012, 2, 64-98.
68. D. Lin, T. Qin, Y. Wang, X. Sun and L. Chen, *ACS Appl. Mater. Interfaces*, 2014, 6, 1320-1329.
69. J. Huang, L. Zhang, B. Chen, N. Ji, F. Chen, Y. Zhang and Z. Zhang, *Nanoscale*, 2010, 2, 2733-2738.
70. X. Huang, H. Li, S. Li, S. Wu, F. Boey, J. Ma and H. Zhang, *Angew. Chem. Int. Edit.*, 2011, 50, 12245-12248.
71. C. Xu, X. Wang and J. Zhu, *J. Phys. Chem. C*, 2008, 112, 19841-19845.
72. F. A. He, J. T. Fan, F. Song, L. M. Zhang and H. L. W. Chan, *Nanoscale*, 2011, 3, 1182-1188.
73. P. Fakhri, M. Nasrollahzadeh and B. Jaleh, *RSC Advances*, 2014, 4, 48691-48697.
74. Z. Zhu, L. Ma, M. Su, D. Liu and Z. Wang, *J. Mater. Chem. B*, 2013, 1, 1432-1438.
75. M. Balcioglu, M. Rana and M. V. Yigit, *J. Mater. Chem. B*, 2013, 1, 6187-6193.
76. U. Dembereldorj, S. Y. Choi, E.-O. Ganbold, N. W. Song, D. Kim, J. Choo, S. Y. Lee, S. Kim and S.-W. Joo, *Photochemistry and Photobiology*, 2014, 90, 659-666.

77. C. M. Xue, M. Gao, Y. H. Xue, L. Zhu, L. M. Dai, A. Urbas and Q. Li, *J. Phys. Chem. C*, 2014, 118, 15332-15338.
78. F. Schedin, E. Lidorikis, A. Lombardo, V. G. Kravets, A. K. Geim, A. N. Grigorenko, K. S. Novoselov and A. C. Ferrari, *ACS Nano*, 2010, 4, 5617-5626.
79. J. B. Lee, S. Shim, B. Kim and H. Suk Chin, *Chem. Eur. J.*, 2011, 17, 2381-2387.
80. T. Maurer, R. Nicolas, G. Lévêque , P. Subramanian, J. Proust, J. Béal, S. Schuermans, J.-P. Vilcot, Z. Herro, M. Kazan, J. Plain, R. Boukherroub, A. Akjouj, B. Djafari-Rouhani, P.-M. Adam and S. Szunerits, *Plasmonics* 2014, 9, 507–512.
81. P. Kundu, C. Nethravathi, P. A. Deshpande, M. Rajamathi, G. Madras and N. Ravishankar, *Chem. Mater.*, 2011, 23, 2772-2780.
82. G. Goncalves, P. A. A. P. Marques, C. M. Granadeiro, H. I. S. Nogueira, M. K. Singh and J. Gracio, *Chem. Mater.*, 2009, 21, 4796-4802.
83. K. Vinodgopal, B. Neppolian, I. V. Lightcap, F. Grieser, M. Ashokkumar and P. V. Kamat, *J. Phys. Chem. Lett.*, 2010, 1, 1987-1993.
84. Y. Li, W. Gao, L. Ci, C. Wang and P. M. Ajayan, *Carbon*, 2010, 48, 1124-1130.
85. S. R. Sahu, M. M. Devi, P. Mukherjee, P. Sen and K. Biswas, *J. Nanomater.*, 2013, 6.
86. P. Zhang, Y. Huang, X. Lu, S. Zhang, J. Li, G. Wei and Z. Su, *Langmuir*, 2014, 30, 8980-8989.
87. S. K. Movahed, M. Fakharian, M. Dabiri and A. Bazgir, *RSC Advances*, 2014, 4, 5243-5247.
88. R. Muszynski, B. Seger and P. V. Kamat, *J. Phys. Chem. C*, 2008, 112, 5263-5266.
89. M. Iliut, C. Leordean, V. Canpean, C.-M. Teodorescu and S. Astilean, *J. Mater. Chem. C*, 2014, 1, 4094-4104.
90. L. Zhou, H. Gu, C. Wang, J. Zhang, M. Lv and R. He, *Colloids and Surfaces A: Physicochemical and Engineering Aspects*, 2013, 430, 103-109.
91. P. Sharma, G. Darabdhara, T. M. Reddy, A. Borah, P. Bezboruah, P. Gogoi, N. Hussain, P. Sengupta and M. R. Das, *Catal. Commun.*, 2013, 40, 139-144.
92. W. L. Fu, S. J. Zhen and C. Z. Huang, *Analyst*, 2013, 138, 3075-3081.
93. Z.-G. Le, Z. Liu, Y. Qian and C. Wang, *Appl. Surf. Sci.*, 2012, 258, 5348-5353.
94. K. Yang, S. Zhang, G. Zhang, X. Sun, S. T. Lee and Z. Liu *Nano Lett.*, 2010, 10, 3318-3323.
95. C. Fu, Y. Kuang, Z. Huang, X. Wang, N. Du, J. Chen and H. Zhou, *Chem. Phys. Lett.*, 2010, 499, 250-253.
96. X.-R. Li, X.-L. Li, M.-C. Xu, J.-J. Xu and H.-Y. Chen, *J. Mater. Chem. A*, 2014, 2, 1697-1703.
97. M. Song, J. Xu and C. Wu, *J. Nanotechnol.*, 2012, 2012, 5.
98. F.-B. Wang, J. Wang, L. Shao, Y. Zhao and X.-H. Xia, *Electrochem. Commun.*, 2014, 38, 82-85.
99. K. Yang, L. Hu, X. Ma, S. Ye, L. Cheng, X. Shi, C. Li, Y. Li and Z. Liu, *Adv. Mater.*, 2012, 24, 1868-1872.
100. M. Iliut, C. Leordean, V. Canpean, C.-M. Teodorescu and S. Astilean, *J. Mater. Chem. C*, 2013, 1, 4094-4104.
101. M. Gkikas, G. V. Theodosopoulos, B. P. Das, M. Tsianou, H. Iatrou and G. Sakellariou, *Euop. Polymer J.*, 2014, 60, 106-113.
102. Y. Wang, S. Zhang, D. Du, Y. Shao, Z. Li, J. Wang, M. H. Engelhard and J. Li, *J. Mater. Chem.*, 2011, 21, 5319-5325.
103. B. S. Kong, J. Geng and H. T. Jung, *Chem. Commun.*, 2009, 2174-2176.
104. M. Du, T. Yang and K. Jiao, *J. Mater. Chem.*, 2010, 20, 9253-9560.
105. Y. C. Fu, P. H. Li, J. Q. Xie, X. H. Xu, L. H. Lei, C. Chen, C. Zou, W. Deng and S. Z. Yao, *Adv. Funct. Mater.*, 2009, 19, 1784-1791.
106. S. Moussa, G. Atkinson, M. SamyEl-Shall, A. Shehata, K. M. AbouZeid and M. B. Mohamed, *J. Mater. Chem.*, 2011, 21, 9608-9619.
107. K. Jasuja and V. Berry, *ACS Nano*, 2009, 3, 2358-2366.
108. Y. Wang, L. Polavarapu and L. M. Liz-Marzan, *ACS Appl. Mater. Interfaces*, 2014, 6, 21798-21805.

109. S. Z. Nergiz, N. Gandra, S. Tadepalli and S. Singamaneni, *ACS Appl. Mater. Interfaces*, 2014, 6, 16395-16402.
110. X. Bian, Z.-L. Song, Y. Qian, W. Gao, Z.-Q. Cheng, L. Chen, H. Liang, D. Ding, X.-K. Nie, Z. Chen and W. Tan, *Sci. Rep.*, 2014, 4, 6093.
111. D.-K. Lim, A. Barhoumi, R. G. Wylie, G. Reznor, R. S. Langer and D. S. Kohane, *Nano Lett.*, 2013, 13, 4075-4079.
112. C. Xu, D. Yang, L. Mei, Q. Li, H. Zhu and T. Wang, *ACS Appl. Mater. Interfaces*, 2013, 5, 12911-12920.
113. Y. Jin, J. Wang, H. Ke, S. Wang and Z. Dai, *Biomaterials*, 2013, 34, 4794-4802.
114. X. Ma, Q. Y. Qu, Y. Zhao, Z. Luo, Y. Zhao, K. W. Ng and Y. L. Zhao, *J. Mater. Chem. B*, 2013, 1, 6495-6500.
115. N. R. Jana, L. Gearheart and C. J. Murphy, *Adv. Mater.*, 2001, 13, 1389-1393.
116. N. R. Jana, L. Gearheart and C. J. Murphy, *J. Phys. Chem. B*, 2001, 105, 4065-4067.
117. N. H. Kim, M. K. Oh, S. Park, S. K. Kim and B. H. Hong, *Bull. Korean Chem. Soc.*, 2010, 31, 999-1003.
118. S. Heeg, R. Fernandez-Garcia, A. Oikonomou, F. Schedin, R. Narula, S. A. Maier, A. Vijayaraghavan and S. Reich, *Nano Lett.*, 2013, 13, 301-308.
119. P. Wang, W. Zhang, O. Liang, M. Pantoja, J. Katzer, T. Schroder and Y. H. Xie, *ACS Nano*, 2012, 6, 6244-6249.
120. W. Xu, J. Xiao, Y. Chen, Y. Chen, X. Ling and J. Zhang, *Adv. Mater.*, 2013, 25, 928-933.
121. W. Xu, X. Ling, J. Xiao, M. S. Dresselhaus, J. Kong, H. Xu, Z. Liu and J. Zhang, *PNAS*, 2012, 109, 9281–9286.
122. A. Reina, X. Jia, J. Ho, D. Nezich, H. Son, V. Bulovic, M. S. Dresselhaus and J. Kong, *Nano Lett.*, 2009, 9, 30-35.
123. K. Sun, J. Y. Lee, B. Y. Li, W. Liu, C. Q. Miao, Y. H. W. Xie, X. Y. and T. P. Russell, *J. Appl. Phys.* , 2010, 108, 036102-036104.
124. H. Shen, L. Zhang, M. Liu and Z. Zhang, *Theranostics*, 2012, 2, 283-294.
125. Z. Liu, J. T. Robinsion, S. M. Tabakman, K. Yang and H. Dai, *Mater. Today*, 2011, 14, 316-323.
126. C. Xu, D. Yang, L. Mei, B. Lu, L. Chen, Q. Li, H. Zhu and T. Wang, *ACS Appl. Mater. Interfaces*, 2013, 10, 2715-2724.
127. Y. Yuan, Y. Zhang, B. Liu, H. Wu, Y. Kang, M. Li, N. He and G. Zhang, *J. Nanobiotechnol.*, 2015, 13, 1-15.
128. E. G. Graham, C. M. MacNeill and N. H. Levi-Polyachenko, *Nano Life*, 2013, 3, 1330002.
129. R. A. Weissleder, *Nat. Biotechnol.*, 2001, 19, 316.
130. O. Akhavan and E. Ghaderi, *ACS Nano*, 2010, 4, 5731-5736.
131. O. Akhavan, E. Ghaderi and A. Akhavan, *Biomaterials*, 2012, 33, 8017-8025.
132. E. Akhavan and E. Ghaderi, *Small*, 2013, 9, 3593-3601.
133. K. Yang, J. Wan, S. Zhang, B. Tian, Y. Zhang and Z. Liu, *Biomaterials*, 2011, 33, 2206-2214.
134. J. T. Robinson, S. M. Tabakman, Y. Liang, H. Wang, H. S. Casalongue, D. Vinh and H. Dai, *J. Am. Chem. Soc.*, 2011, 133, 6825-6831.
135. X. Huang, P. K. Jain, I. H. El-Sayed and M. A. El-Sayed, *Lasers Med. Sci.*, 2008, 23, 217-228.
136. P. C. Ray, S. A. Khan, A. K. Singh, S. D. and Z. Fan, *Chem. Soc. Rev.*, 2012, 41, 3193-3209.
137. S. Z. Nergiz, N. Gandra, S. Tadepalli and S. Singamaneni, *ACS Appl. Mater. Interfaces*, 2014, 6, 16395-16402.
138. A. F. Zedan, S. Moussa, J. Terner, G. Atkinson and M. S. El-Shall, *ACSNano*, 2013, 7, 627.
139. L. Yang, Y.-T. Tseng, G. Suo, L. Che, J. Yu, W.-J. Choi, C.-C. Huang and C.-H. Lin, *ACS Appl. Mater. Interfaces*, 2015, 7, 5097-5106.

140. D. Lin, T. Quin, Y. Wang, X. Sun and L. Chen, *ACS Appl. Mater. Interfaces*, 2014, 6, 1320-1329.
141. K. R. Ratinac, W. J. Yang, J. J. Gooding, P. Thordarson and F. Braet, *Electroanalysis*, 2011, 23, 803-826.
142. H. J. Jiang, *Small*, 2011, 7, 2413-2427.
143. S. J. Guo and S. J. Dong, *Chem. Soc. Rev.*, 2011, 40, 2644-2672.
144. D. Chen, L. Tang and J. Li, *Chem. Soc. Rev.*, 2010, 39, 3157-3180.
145. L. Tang, Y. Wang, Y. Li, H. Feng, J. Lu and J. Li, *Adv. Funct. Mater.*, 2009, 19, 2782-2789.
146. C. S. Shan, H. F. Yang, D. X. Han, Q. Zhang, A. Ivaska and L. Niu, *Biosens. and Bioelect.*, 2010, 25, 1070-1074.
147. Y. Fang, S. Guo, C. Zhu, Y. Zhai and E. Wang, *Langmuir*, 2010, 26, 11277-11282.
148. H. Chang, X. Wang, K. K. Shiu, Y. Zhu, J. Wang, Q. Li, B. Chen and H. Jiang, *Biosens. and Bioelect.*, 2013, 41, 789-794.
149. Z. Wang, J. Zhang, Z. Yin, S. Wu, D. Mandler and H. Zhang, *Nanoscale*, 2012, 4, 2728-2733.
150. H.-P. Peng, Y. Hu, P. Liu, Y.-N. Deng, P. Wang, W. Chen, A.-L. Liu, Y.-Z. Che and X.-H. Lin, *Sen. Actuators B*, 2015, 207, 269-276.
151. Q. Wang, Q. Wang, M. Li, S. Szunerits and R. Boukherroub, *unpublished results*.
152. Y. Yu, Z. Chen, S. He, B. Zhang, X. Li and M. Yao, *Biosens. and Bioelect.*, 2014, 52, 147-152.
153. V. K. Gupta, N. Atar, M. L. Yola, M. Eryilmaz, H. Torul, U. Tamer, I. H. Boyaci and Z. Ustundag, *J. Colloid Interf. Sci.*, 2013, 406, 231-237.
154. J. Ju and W. Chen, *Anal. Chem.*, 2014, 87, 1903-1910.
155. Y. Xue, H. Zhao, Z. Wu, X. Li, Y. He and Z. Yuan, *Biosens. and Bioelect.*, 2011, 29, 102-108.
156. O. Parlak, A. Tiwari, A. P. F. Turner and A. Tiwari, *Biosens. and Bioelect.*, 2013, 49, 53-62.
157. J. Liang, Z. Chen, L. Guo and L. Li, *Chem. Commun.*, 2011, 47, 5476-5478.
158. S. Azzouzi, L. Rotariu, A. M. Benito, W. K. Maser, M. Ben Ali and C. Bala, *Biosen. Bioelectron.*, 2015, 69, 208-286.
159. L. Wang, E. Hua, M. Liang, C.-C. M. Ma, Z. Liu, S. Sheng, M. Liu, G. Xie and W. Feng, *Biosens. and Bioelect.*, 2014, 51, 201-207.
160. Z. Chen, C. Zhang, X. Li, H. Ma, C. Wang, K. Li and Y. Lin, *Biosen. Bioelectron.*, 2015, 65, 232-237.
161. Z. Zhong, W. Wu, D. Wang, D. Wang, J. Shan, Y. Qing and Z. Zhang, *Biosens. and Bioelect.*, 2010, 25, 2379-2383.
162. Q. Wei, Z. Xiang, J. He, G. Wang, H. Li, Z. Qian and M. Yang, *Biosens. and Bioelect.*, 2010, 26, 627-631.
163. J. Zhang, Y. P. Sun, B. Xu, H. Zhang, Y. Gao and D. Song, *Biosens. and Bioelect.*, 2013, 45, 230-236.
164. F. Yang, Z. Yang, Y. Zhuo, Y. Chai and R. Yuan, *Biosen. Bioelectron.*, 2015, 66, 356-362.
165. L. Wang, M. Xu, L. Han, M. Zhou, C. Zhu and S. Dong, *Anal. Chem.*, 2012, 84, 7301-7307.
166. X. Sun, J. Ji, D. Jiang, X. Li, Y. Zhang, Z. Li and Y. Wu, *Biosens. and Bioelect.*, 2013, 44, 122-126.
167. S. Mao, G. Lu, K. Yu, Z. Bo and J. Chen, *Adv. Mater.*, 2010, 22, 3521-3526.
168. K. Kneipp, Y. Wang, H. Kneipp, L. T. Perelman, I. Itzkan, R. R. Dasari and M. S. Feld, *Phys. Rev. Lett.*, 1997, 78, 1667.
169. S. Nie and S. R. Emory, *Science*, 1997, 275, 1102-1106.
170. S. Sun and P. Wu, *Phys. Chem. Chem. Phys.*, 2011, 13, 21116-21120.
171. G. Das, N. Patra, A. Gopalakrishnan, R. P. Zaccaria, A. Toma, S. Thorat, E. Di Fabrizio, A. Diaspro and M. Salerno, *Analyst*, 2012, 137, 1785-1792.

172. M. Li, J. Zhang, S. Suri, L. J. Sooter, D. Ma and N. Wu, *Anal. Chem.*, 2012, 84, 2837-2842.
173. P. Alivisatos, *Nature biotechnology*, 2003, 22, 47-52.
174. Y. C. Cao, R. Jin and C. A. Mirkin, *Science*, 2002, 297, 1536-1540.
175. J. Yang, M. Palla, F. G. Bosco, T. Rindzevicius, T. S. Alstrom, M. S. Schmidt, A. Boisen, J. Ju and Q. Lin, *ACS Nano*, 2013, 7, 5350-5359.
176. D. Lin, S. Feng, H. Huang, W. Chen, H. Shi, N. Liu, L. Chen, W. Chen, Y. Yu and R. Chen, *J. Biomed. Nanotechnol.*, 2012, 10, 478-484.
177. X. Qian, X.-H. Peng, D. O. Ansari, Q. Yin-Goen, G. Z. Chen, D. M. Shin, L. Yang, A. N. Young, M. D. Wang and S. Nie, *Nat. Biotechnol.*, 2007, 26, 83-90.
178. C. Zavaleta, A. De La Zerda, Z. Liu, S. Keren, Z. Cheng, M. Schipper, X. Chen, H. Dai and S. S. Gambhir, *Nano Lett.*, 2008, 8, 2800-2805.
179. T. H. Kim, K. B. Lee and J. W. Choi, *Biomaterials*, 2013, 34, 8660-8670.
180. X.-M. Lin, Y. Cui, Y.-H. Xu, B. Ren and Z.-Q. Tian, *Anal. Bioanal. Chem.*, 2009, 394, 1729-1745.
181. X. Ling, L. Xie, Y. Fang, H. Xu, H.-L. Zhang, J. Kong, M. S. Dresselhaus, J. L. Zhang and Z. Liu, *Nano Lett.*, 2010, 10, 553-561.
182. X. Yu, H. Cai, W. Zhang, X. Li, N. Pan, Y. Luo, X. Wang and J. G. Hou, *ACS Nano*, 2011, 5, 952-958.
183. K. Jasuja, J. Linn, S. Melton and V. Berry, *J. Phys. Chem. Lett.*, 2010, 1, 1853-1860.
184. G. Lu, H. Li, C. Liusman, Z. Yin, S. Wu and H. Zhang, *Chem. Sci.*, 2011, 2, 1817-1821.
185. C. Hu, J. Rong, J. Cui, Y. Yang, L. Yang, Y. Wang and Y. Liu, *Carbon*, 51, 255-264.
186. Q. Liu, L. Wei, J. L. Wang, F. Peng, D. Luo, R. Cui, Y. Niu, X. Qin, Y. Liu, H. Sun, J. Yang and Y. Li, *Nanoscale*, 2012, 4, 7084-7089.
187. Z. Liu, C. Hu, S. Li, W. Zhang and Z. Guo, *Anal. Chem.*, 2012, 84, 10338-10344.
188. J. Huang, C. Zong, H. Shen, M. Liu, B. Chen, B. Ren and Z. Zhang, *Small*, 2012, 16, 2577-2584.
189. Y. K. Kim, H. K. Na, S. Kim, H. Jang, S. J. Chang and D. H. Min, *Small*, 2015, doi: 10.1002/smll.201402269.
190. Y. Cao, Y. Ma, M. Zhang, H. Wang, X. Tu, H. Shen, J. Dai, H. Guo and Z. Zhang, *Adv. Funct. Mater.*, 2014, 24, 6963-6971.